9748

FAIRCHILD HILLER
REPUBLIC AVIATION DIVISION
FARMINGDALE, LONG ISLAND, NEW YORK

NASA CR ___________

FINAL REPORT

Prepared for:

George C. Marshall Space Flight Center
National Aeronautics and Space Administration
Huntsville, Alabama 35812

Contract: NAS 8-20663

For Period: August, 1966 - September, 1969

Prepared by:

Gerald Levy
Leon Zadoff
Martin Begun

FAIRCHILD HILLER CORPORATION
REPUBLIC AVIATION DIVISION
Power Conversion Department
Farmingdale, New York 11735

PCD-TR-69-6
FHR 3287-3
PC090R0003

Measurement of Electric Fields
In The Ionosphere

FINAL REPORT

Contract: NAS 8-20663
September, 1969

CONTENTS

FOREWORD

This report describes the continuation of the development of an experimental laboratory model of an electric field meter using the electron beam deflection technique and the development of a glow discharge test chamber within which laboratory testing of this meter in an ionized environment was accomplished.

This effort was supported by the Space Science Laboratory of George C. Marshall Space Flight Center under the technical management of Mr. E.L. Shriver.

The facilities of the Republic Aviation Division of Fairchild Hiller Corporation, Power Conversion Department which is under the direction of Mr. A.E. Kunen, were made available for this work.

The project investigator was Mr. G. Levy. The principal physicist was Dr. L. Zadoff and the experimental physicist was Mr. M. Begun. Major contributions to this program were made by Mr. A. Urban, project designer, Mr. H. Jacobs, instrumentation engineer, and Mr. J. Porte, performing the analog computer analysis. The cooperation and support of the laboratory staff under the direction of Mr. L. Brown is gratefully acknowledged.

This work was performed as a continuation of National Aeronautics and Space Administration contract NAS 8-20663. The final report under the preceding phase is NASA CR-61189 dated January, 1968. This final report is Fairchild Hiller Corporation Report No. PCD-TR-69-6, FHR 3287-3, PC090R0003, dated September, 1969.

ABSTRACT

This report describes the continuation of the development of an experimental laboratory model of an electric field meter using the electron beam deflection technique and the development of a glow discharge test chamber within which laboratory testing of this meter in an ionized environment was accomplished.

SECTION I

INTRODUCTION

When one considers measuring electric fields that exist within the Earth's ionosphere, immediately one is faced with a myriad of problems. These problems range from the fact that an apparent electric field ($\bar{v} \times \bar{B}$) of a maximum of 300 millivolts/meter is measured reflecting the velocity of the vehicle on which the meter is being transported across the Earth's magnetic field; to the plasma properties of the ionosphere in which the electric field to be measured exists.

Experiments have been flown which demonstrated that an ambient electric field does indeed exist, however, a more tractable method for measuring electric field strength within the ionosphere is needed.

In addition to the ambient electric field within the ionosphere, and the apparent electric field due to the relative motion of the meter with respect to the ionosphere; electric fields exist due to charge separation caused by the motion of the spacecraft through the ionospheric plasma. These plasma sheath fields are extremely strong near the body (in the order of 500 volts/meter at 700 km altitude), and vary significantly depending upon position about the body. Both the ambient and induced electric fields have import in the understanding of the magnetosphere and in the design and operation of spacecraft operating within the ionosphere.

Therefore, it is desirable to develop an electric field meter capable of measuring precisely the relatively weak ambient electric fields (which have been measured to vary from 2 millivolt/meter to 85 millivolt/meter) in the presence of the apparent ($\bar{v} \times \bar{B}$) electric field while having the dynamic range to measure the extremely strong fields due to plasma sheaths. The measurement of these electric fields will require sophisticated instrumentation and experimental techniques. The meter used must not modify the electric field being measured. This means that there should be no modification of the environment by the meter, while at the same time the electric field must influence the field sensing portion of the meter. The meter must also be immune to the effects of extraneous noise produced by such agencies as charge particle bombardment, secondary emission by electromagnetic radiation, RF excitation, and cosmic radiation. The environment must also be considered. It must be free of artificially created electric fields. This means that electric field producing experiments and functional spacecraft devices must be properly shielded.

The variety of methods to measure the electric field within the ionosphere that have been used include: electrostatic probes, field mill, and charged particle deflection. Experiments using the probe type of meter were reported by Gdalevich and Imyanitov[1], and Muzer and Bruston[2]. An excellent analysis of the design and limitations of electrostatic probe measurement within the ionosphere is given by Fahleson[3]. The field mill meter within the ionosphere is limited by the plasma sheath currents. Lafferty[4] discussed the results of an induced charge experiment flown on Gemini IV and V missions. Wildman[5] has reported a field mill design which may improve electric field measurements within the ionosphere for this type of instrumentation.

Perhaps the most interesting measurements of ambient electric fields within the ionosphere were reported by Haser[6]. In this experiment clouds of barium and strontium vapors were released in the ionosphere. The barium is rapidly ionized by the sun and tends to diffuse along the magnetic field lines forming long narrow streamers. The strontium is not ionized and it retains a globular shape. The rate of separation of these two clouds provides a measurement of the electric field strength. The dynamical model of the interaction of electric and magnetic fields within the ionized cloud and the charged particles is still being studied.

The concept of measuring the deflection of a beam of charged particles when introduced into an electric field is not new, R.W. Warren, "Measurement of Electric Fields as Applied to Glow Discharges," Rev. Sci. Inst., August, 1955[7] discussed its use. However, the technique has not been widely used for this purpose. For this reason in 1964 the Research Projects Laboratory of the George C. Marshall Space Flight Center, Huntsville, Alabama, began an investigation to determine if this technique might be used to measure electric field strengths encountered in space exploration. The results of this effort, using a sensitive but rather uncomplicated meter, showed that fields of 1 volt per meter could be easily measured in the laboratory. Indeed it was apparent that a program of development and optimization would yield a much more sensitive instrument which should have application in the space exploration program. This work was reported in NASA TMX 53435, "Investigation of the Deflection of an Electron Beam as a Means of Measuring Electric Field Strength," April 12, 1966 by E. L. Shriver[8]. In August, 1966, a contract was established by the NASA/MSFC with Fairchild Hiller Corporation, Republic Aviation Division, for the development of a field meter of this type. These efforts have produced an experimental model electric field meter using the deflection of an electron beam as a means of measuring electric field strength. The spacecraft field meter systems concept necessary for the operation of this meter in the ionosphere have also been investigaed. The field meter which has been developed uses a low current electron beam (less than one microampere) to provide a field sensing element which does not disturb the environment or the field being measured. It may be used to measure electric fields at desired locations relative to the spacecraft both near and far from the spacecraft surface[9].

The next task performed in the development of this instrument was to test the instrument in an ionized environment. The complete simulation of the ionosphere in the laboratory is a formidable problem beyond the scope of our development. A glow discharge has been generated which provides, in its positive column, an electric field existing within the ionized gas. Some aspects of the operation of the field meter in the ionosphere have been simulated closely enough to provide meaningful test results.

Section II of this report presents results of electrical Faraday cage analysis and simulations for both electrostatic and electrodynamic cases with linear current and voltage relationships. The preliminary design of a mechanical cage is also presented. The performance of the electron beam and deflection loops as a function of pressures are presented in Section III. The description of the glow discharge chamber, the double Langmuir probe, and the measurements of the plasma and electric field parameters as a function of pressure and discharge conditions are presented in Section IV. Included in the Appendices is an analysis of the electron beam-neutral gas interactions with and without an electric field.

SECTION II

FARADAY CAGE DESIGN

A. INTRODUCTION

One of the unique concepts in the design of the electron beam electric field meter is the chopping of the electric field. This chopping technique permits the discrimination between the deflection of electrons caused by the motion through the earth's magnetic field and that caused by an electric field. The Faraday cage is a device which shields electric fields from penetrating into the region in which the electron beam exists.

Since it would be advantageous if a cage could be designed to open and close without mechanical devices, the possibilities of utilizing the ionospheric properties to open and close the cage electrically were explored.

In concept, the electrical Faraday cage consists of an array of wires so arranged about the electron beam that when these wires are electrically isolated from each other, the electric field penetrates undistorted to the electron beam. Then, when these wires are electrically shorted to each other, the electric field is shielded from the electron beam.

This section relates the analysis, analog simulation and design of the Faraday cage.

B. ANALYSIS OF ELECTRIC FIELD DISTORTION BY A CIRCULAR ARRAY OF LONG METAL WIRES

A number of long cylindrical metal wires are arranged around the circumference of a circle whose plane is perpendicular to the wires. There is a uniform external electric field whose direction is also perpendicular to the wires. It is desired to find the distortion of the external field caused by the presence of the wires at the center of the circular array.

If we consider only one cylindrical wire in a uniform external field, the potential Ψ, external to the wire, is given by:

$$\Psi = -Er\cos\varphi + E\left(\frac{a^2}{r}\right)\cos\varphi \qquad 1$$

where r and φ are the polar coordinates whose origin is at the center of the circular cross-section of the wire, and the field of magnitude E is in the x direction. The radius of the wire is a. The first term on the right is the uniform field, while the second term is the distortion due to the presence of the wire. The appearance of this term is that of the potential of a dipole. This dipole is induced by the redistribution of charge about the periphery of the metallic cylinder to exclude the field from its interior. It may be noted that for a fixed r, the distortion is proportional to a^2.

We shall first treat the circular array of wires by making the approximation that the ratio of wire radius to spacing is sufficiently small that electric field produced by each wire is unaffected by the presence of the other wires. Consequently, the field distortion at the center of the array is obtained by superposition of the field produced by the presence of the individual wires. Then we shall examine the error resulting from neglect of the interaction between wires. This interaction occurs from the redistribution of charges on each wire, not only due to the presence of the external uniform field, but also as a result of the fields of the other wires.

In cartesian coordinates the potential for a single wire is:

$$\Psi = Ex\left(-1 + \frac{a^2}{x^2 + y^2}\right) \tag{2}$$

and the field is:

$$\underline{E} = \underline{a}_x E\left[1 - \frac{a^2(x^2 - y^2)}{(x^2 + y^2)^2}\right] + \underline{a}_y E \frac{2a^2xy}{(x^2 + y^2)^2} \tag{3}$$

where $\underline{a}_x$ and $\underline{a}_y$ are unit vectors in the x and y directions respectively. It may be noted that if we subtract $\underline{a}_x E$ from Equation (3) the remainder is the distortion produced by the wire.

Let us now calculate the distortion produced at the center of the array, using the superposition approximation.

$$\underline{E} = \underline{a}_x E a^2 \sum_{j=1}^{N} \frac{x_j^2 - y_j^2}{(x_j^2 + y_j^2)^2} + \underline{a}_y E a^2 \sum_{j=1}^{N} \frac{2x_j y_j}{(x_j^2 + y_j^2)^2} \tag{4}$$

The total number of wires is N and x_j, y_j are the x and y coordinates of the center of the array for an origin of the j^{th} wire. Let R be the radius of the circular array and let α be the angle made with the electric field direction by a line joining the center of the wire nearest the positive x axis. It is convenient to label this wire number 1 and count the remainder in a counterclockwise fashion. Then,

$$x_j = R\cos\left(j\frac{2\pi}{N}+\alpha\right)$$
$$y_j = R\sin\left(j\frac{2\pi}{N}+\alpha\right) \qquad 5$$

and Equation (4) becomes:

$$\underline{E} = \underline{a}_x E\left(\frac{a}{R}\right)^2 \sum_{j=1}^{N} \cos\left(j\frac{4\pi}{N}+2\alpha\right) + \underline{a}_y E\left(\frac{a}{R}\right)^2 \sum_{j=1}^{N} \sin\left(j\frac{4\pi}{N}+2\alpha\right). \qquad 6$$

But,

$$\sum_{j=1}^{N} \cos\left(j\frac{4\pi}{N}+2\alpha\right) = \cos 2\alpha \sum_{j=1}^{N} \cos\left(j\frac{4\pi}{N}\right) - \sin 2\alpha \sum_{j=1}^{N} \sin\left(j\frac{j4\pi}{N}\right) \qquad 7$$

and,

$$\sum_{j=1}^{N} \sin\left(j\frac{4\pi}{N}+2\alpha\right) = \sin 2\alpha \sum_{j=1}^{N} \cos\left(j\frac{4\pi}{N}\right) + \cos 2\alpha \sum_{j=1}^{N} \sin\left(j\frac{4\pi}{N}\right). \qquad 8$$

An interesting special case arises when the number of wires is divisible by four. Then we may let N = 4n where N is an integer. The summation then takes on the value:

$$\sum_{j=1}^{N} \cos\left(j\frac{4\pi}{N}\right) = \sum_{j=1}^{4n} \cos\frac{j\pi}{n}$$
$$= \sum_{j=1}^{n} \cos\left(j\frac{\pi}{n}\right) + \sum_{j=n+1}^{2n} \cos\left(j\frac{\pi}{n}\right) + \sum_{j=2n+1}^{3n} \cos\left(j\frac{\pi}{n}\right)$$
$$+ \sum_{j=3n+1}^{4n} \cos\left(j\frac{\pi}{n}\right)$$

Now consider:

$$\sum_{j=n+1}^{2n} \cos\left(j\frac{\pi}{n}\right)$$

Let $j = k + n$. Then,

$$\sum_{j=n+1}^{2n} \cos\left(j\frac{\pi}{n}\right) = \sum_{k=1}^{n} \cos\left[\frac{(k+n)\pi}{n}\right] = \sum_{k=1}^{n} \cos\left[\left(\frac{k\pi}{n}\right) + \pi\right]$$

$$= -\sum_{k=1}^{n} \cos\left(\frac{k\pi}{n}\right)$$

Similarly,

$$\sum_{j=2n+1}^{3n} = \sum_{k=1}^{n} \cos\left(\frac{k\pi}{n}\right)$$

and,

$$\sum_{j=3n+1}^{4n} \cos\left(\frac{j\pi}{n}\right) = -\sum_{k=1}^{n} \cos\left(\frac{k\pi}{n}\right)$$

Finally, then, for $N = 4n$

$$\sum_{j=1}^{N} \cos\left(j\frac{4\pi}{N}\right) = 0$$

Similarly, for $N = 4n$

$$\sum_{j=1}^{N} \sin\left(j\frac{4\pi}{N}\right) = 0$$

Hence within the limitations of the superposition approximation, the field distortion at the center of the array for a number divisible by four is zero. Since this result occurs because of cancellation of fields when the wires are regularly spaced, any departure from regularity will result in some field distortion. Completely random orientation of the wires would lead to field components of the order of $\sqrt{N}\ E\,(a/R)^2$.

We next evaluate the accuracy of the superposition approximation. We do this by considering the next order approximation. Let us focus attention on one wire and consider the fields produced by the other wires at the location of the wire under scrutiny. We again use the superposition approximation to do this. Next, since the wire radius is assumed small compared to the spacing, we shall assume that the effect of this superposition will be a field which is uniform over the dimensions of the wire. We add this field to the original external field were present. The distortion of the x component of the field would then be calculated from Equation (3) with $E + E_c$ substituted for E where E_c is the correction to the original field. Now E_c is evidently of the order of $E(a/\rho)^2$ where ρ is the spacing between wires.

Thus the error introduced by the neglect of the interaction is of the order of $E a^4/\rho^2 R^2$. For a typical cage of R = 4 inches, ρ = 0.5 inches and a = 0.005 inches, the error is 10^{-12} of the ambient electric field E.

Further, this analysis can be applied to electric fields which are not perpendicular to the wires; if only the electric field components which are perpendicular are considered. Thus for any electric field orientation the circular array consisting of a multiple of 4 wires, will have a most probable distortion at the center of the array of $\sqrt{N}\, E\, (a/R)^2$ if the location of each wire is randomly placed about the periphery of the circle. For N = 88 and the same a and R as above, the distortion is 10^{-5} of the ambient field E.

C. SHIELDING BY A CIRCULAR ARRAY OF CONDUCTING WIRES IN A UNIFORM EXTERNAL FIELD

We consider here an array of infinitely long parallel conducting wires placed uniformly about the circumference of a circle which lies in a plane perpendicular to the wires. The array of wires is placed in a uniform electric field whose direction is perpendicular to the wires. It is desired to find the electric field in the center of the array when the wires are electrically connected so that all the wires are at the same potential. We will consider the special case of the number of wires N to be divisible by four and so oriented that the wires may be selected in pairs lying on a line parallel to the electric field direction.

We will let the wire radius be a and the radius of the circular array be R. The external electric field is to be oriented in the positive x direction.

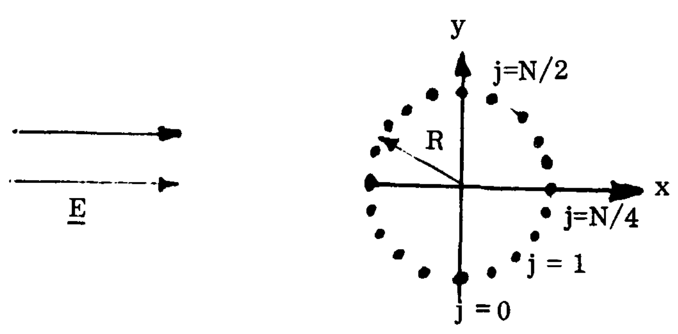

The magnitude of the external field is E. Finally we provide each wire with an index k, letting $k = 0$ at $x = 0$, $y = -R$ and counting counter-clockwise. The wire at $x = R$, $y = 0$ is then N/4 and the one at $x = 0$, $y = R$ is N/2. The units used in the treatment will be e.s.u., although the final results will be obtained in terms of dimensionless ratios.

When the unconnected wires are placed in the external field, the charges redistribute themselves about the wire, so that a dipole moment per unit length is acquired although the net charge per wire remains zero. However, when the wires are connected together, the individual wires acquire charges, although the total charge of the system of charges is zero. For a field oriented as shown, the wires $j = (N/2) + 1$ to $j = N - 1$ acquire a negative charge; the wires $j = 1$ to $(N/2)-1$ acquire a positive charge; while wires $j = 0$ and $j = N/2$ have no charge. This results from the fact that when shorted together with the wires acquire charges which tend to cancel the field at the center of the array. (The external field pushes the positive charges from the left side of the array to the right side).

The potential V at any point is then

$$V = -Ex + \sum_{j=0}^{N/2} \lambda_j \ln \frac{(x + x_j)^2 + (y - y_j)^2}{(x - x_j)^2 + (y - y_j)^2} \tag{9}$$

where (x_j, y_j) are the coordinates of the j^{th} wire. The λ_j's are the magnitude of the charge per unit length of the j^{th} wire. When $x = x_k$, $V = 0$

$$0 = -Ex_k + \sum_{\substack{j=0 \\ j \neq k}}^{N/2} \lambda_j \ln \frac{(x_k + x_j)^2 + (y_k - y_j)^2}{(x_k - x_j)^2 + (y_k - y_j)^2} + \lambda_k \ln\left(\frac{2x_k}{a}\right)^2 \tag{10}$$

The wire locations are

$$x_j = R \sin j \frac{2\pi}{N}$$

$$y_j = -R \cos j \frac{2\pi}{N} \tag{11}$$

The last term at the right of Equation (10) appears since the expression in Equation (9) is valid only outside the wires, the potential being constant inside the wires. Also, the wires are assumed sufficiently small so that the potential is the same as if the charges were concentrated at the center of the wires. By making substitution of Equation(11) into Equation(10), we obtain, after some manipulation,

$$0 = \frac{Ex_k}{2} + \sum_{\substack{j=0 \\ j\neq k}}^{N/2} \lambda_j \ln \frac{\sin(j+k)\frac{\pi}{N}}{\left|\sin(j-k)\frac{\pi}{N}\right|} + \lambda_k \ln\left(\frac{2x_k}{a}\right) \qquad 12$$

Equation(12) constitutes the N/2 linear algebraic equations for the unknowns λ_k. This can in principle be solved since the coefficients are known. However, an excellent approximation, for the number of wires N being large, can be obtained by making the assumption that the value of the charge per unit length is given by

$$\lambda_j = \lambda_{N/4} \sin \frac{2\pi j}{N} \qquad 13$$

The conditions under which this assumption is valid is discussed in the appendix. Then after making the substitution in Equation(12) and taking k = N/4, we obtain

$$0 = \frac{-ER}{2} + \lambda_{N/4} \sum_{\substack{j=0 \\ j\neq N/4}}^{N/2} \sin\frac{2\pi j}{N} \ln \frac{\sin(j+\frac{N}{4})\frac{\pi}{N}}{\left|\sin(j-\frac{N}{4})\frac{\pi}{N}\right|} + \lambda_{N/4} \ln\left(\frac{2R}{a}\right)$$

Solving for $\lambda_{N/4}$, we get

$$\lambda_{N/4} = \frac{ER}{2\left[\sum\limits_{\substack{j=0 \\ j\neq N/4}}^{N/2} \sin\frac{2\pi j}{N} \ln \frac{\sin(j+\frac{N}{4})\frac{\pi}{N}}{\left|\sin(j-\frac{N}{4})\frac{\pi}{N}\right|} + \ln\left(\frac{2R}{a}\right)\right]} \qquad 14$$

Provided that the assumption of Equation(13) is correct we then have the values of all the λ_j.

If we know the values of the λ_j, the calculation of the net electric field at the center of the array is straightforward. From Equation (9)

$$E_x = -\frac{\partial V}{\partial x} = E - \sum_{j=0}^{N/2} 4\lambda_j \frac{x_j\left[(x_j^2 - x^2) + (y-y_j)^2\right]}{\left[(x-x_j)^2 + (y-y_j)^2\right]\left[(x+x_j)^2 + (y-y_j)^2\right]} \qquad 15$$

at the center (0,0)

$$E_x = E - \sum_{j=0}^{N/2} 4\lambda_j x_j \frac{1}{x_j^2 + y_j^2} \tag{16}$$

But

$$x_j^2 + y_j^2 = R^2 \tag{17}$$

$$\therefore E_x = E - \frac{4\lambda_{N/4}}{R} \sum_{j=0}^{N/2} \sin^2 \frac{2j\pi}{N} \tag{18}$$

The summation in Equation(14), $\Sigma_{N/4}$, can be approximated by integrals, in terms of which

$$\Sigma_{N/4} \simeq \frac{N}{\pi} \left[- \int_{\pi/4}^{3\pi/4} \cos 2s \ln sds - \int_{\pi/N}^{\pi/4} \cos 2s \ln \sin sds \right]$$

$$\simeq \frac{N}{\pi} \left[\frac{\pi}{2} + \sin \frac{2\pi}{N} (\ln \sin \frac{\pi}{N} - \tfrac{1}{2}) + \frac{\pi}{N} \right] \tag{19}$$

If we neglect terms of $0(1/N)$ compared to terms of $0(1)$, then,

$$\Sigma_{N/4} \simeq \frac{N}{2} \tag{20}$$

This result is a special case of the more general summation treated in Appendix II. Substitution in Equation(14) yields

$$\lambda_{N/4} = \frac{ER}{N + 2 \ln\left(\frac{2R}{a}\right)} \tag{21}$$

Then Equation (18) becomes

$$E_x = E \left[1 - \frac{4 \sum_{j=0}^{N/2} \sin^2 2j \frac{\pi}{N}}{N + 2 \ln \left(\frac{2R}{a}\right)} \right] \tag{22}$$

Again using an integral to approximate the summation in Equation (22)

$$\sum_{j=0}^{N/2} \sin^2 \frac{2j\pi}{N} \simeq \frac{N}{4} \qquad 23$$

Finally

$$E_x \simeq E \left[1 - \frac{1}{1 + \frac{2}{N} \ln \left(\frac{2R}{a} \right)} \right] \qquad 24$$

Thus the term

$$S = \frac{1}{1 + \frac{2}{N} \ln \left(\frac{2R}{a} \right)} \qquad 25$$

can be used as a figure of merit to represent the effectiveness of shielding at the center of the array. We note that as N gets large S approaches 100%. It may be noted that the chosen orientation of the array relative to the field is not significant since the field may be resolved into two components each of which has the orientation chosen in the analysis.

D. INTERMITTENT FARADAY CAGE ANALOG SIMULATION

We are pursuing two approaches to provide the chopping of the electric field. Within the F region of the ionosphere we are designing an electrically intermittent Faraday cage; while in the other regions of space mechanical operation is required. The possibility of an electrically operated Faraday cage is extremely tantalizing, since it eliminates the requirement for moving parts. The concept is an arrangement of conductors symmetrically located around the electron beam. When these conductors are floating at least 99% of the ambient field is present within the Faraday cage to deflect the beam, and when the conductors are shorted together at least 99% of the ambient field is shielded from the beam.

The problems involved in this development are:

1. When the cage is open the ambient electric field must not be distorted by the presence of the floating conductors.
2. When the cage is closed, the ambient field must be adequately shielded out.
3. When the cage is re-opened on the cyclical basis, the charges on the conductors must redistribute through the ionospheric plasma suffiently fast so that the ambient field is re-established at the electron beam location in a time much shorter than the chopping frequency.

To design a Faraday cage to meet the open and short requirements, two dimensional analog simulation of a variety of conductor configurations were run. The EAI analog computer model number 231R and variplotters model number 1100E were used to follow specific potential lines. Resistance paper of 8000 ohms per square was used to establish the field between electrodes painted on the paper with silver conducting paint.

The potential lines in the center of the paper were plotted and used as the reference field. Then the conductors were painted on in accordance with the two dimensional end view of the cage being studied. The potential lines in the center were again plotted. Comparison of the potential lines before and after the end view conductors were painted on the papers provided data on the amount of distortion created by the presence of the conductors. Then the conductors were shorted together by shielded wires out of the plane of the paper. The center potential lines were again plotted. A comparison of the potential lines before the conductors were painted on and those after the conductors were shorted together by shielded wires out of the plane of the paper. The center potential lines were again plotted. A comparison of the potential lines before the conductors were painted on and those after the conductors were shorted indicates the amount of shielding that the cage provides. Table I indicates the results of a number of configurations. Figure 1 shows the analog computer, the model on the variplotter and some potential lines which were plotted, while Figure 2 is a close-up of the variplotter and the simulated cage.

E. THREE DIMENSIONAL TESTS OF FARADAY CAGE AT S.T.P.

The assembled Faraday cage was placed between two 4 ft. x 4 ft. aluminum sheets. A potential was applied between the sheets creating an electric field at the Faraday cage. A two wire probe was placed at the center of the cage to measure the electric field.

The field was produced by applying simusoidal voltages across the aluminum sheet, the outputs of the wire probes were applied to a differential amplifier and displayed on an oscilloscope along with the applied voltage for synchronization and comparison.

Comparison of the developed voltage across the probe when it was placed within an open (wires electrically isolated) cage and on the probe with the cage removed showed approximately the same field. This indicated that the presence of the cage negligibly distorted the electric field in its center.

TABLE I. ANALOG SIMULATION RESULTS OF ELECTRICAL FARADAY CAGE

Configuration	Rectangular Plates 5-½" Long 6" Separation	Rectangular Plates 5-½" Long 7" Separation	Circular Slats 7" Diameter ½" w. 1" Separation	Circular Slats 7" Diameter 1" w. ½" Separation	Circular Wires Single Circle 7" Dia. 1" Separation	Circular Wires Single Circle 7" Dia. ½" Separation	Circular Wires Single Circle 7" Dia. ¼" Separation	Circular Wires Two Circles 7" and 8" Dia. ½" Spacing, Interspersed
Ambient E Field % Distortion	46%	25%	5%	9%	<1%	<1%	<1%	<1%
Ambient E Field % Shielding	>99%	>99%	86%	95%	84%	96%	99%	>99%

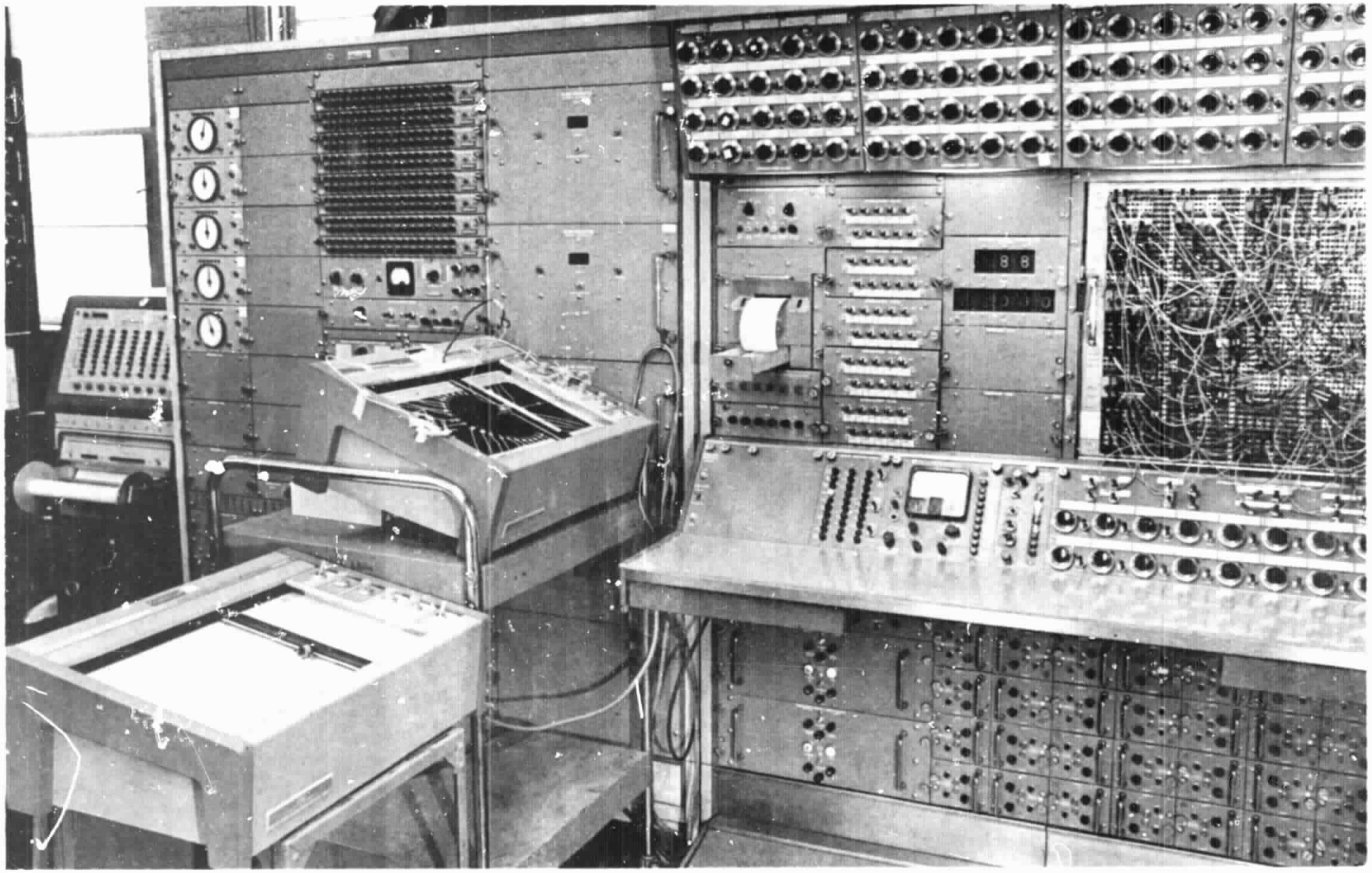

Figure 1. Analog Simulation of Electrostatic Problem

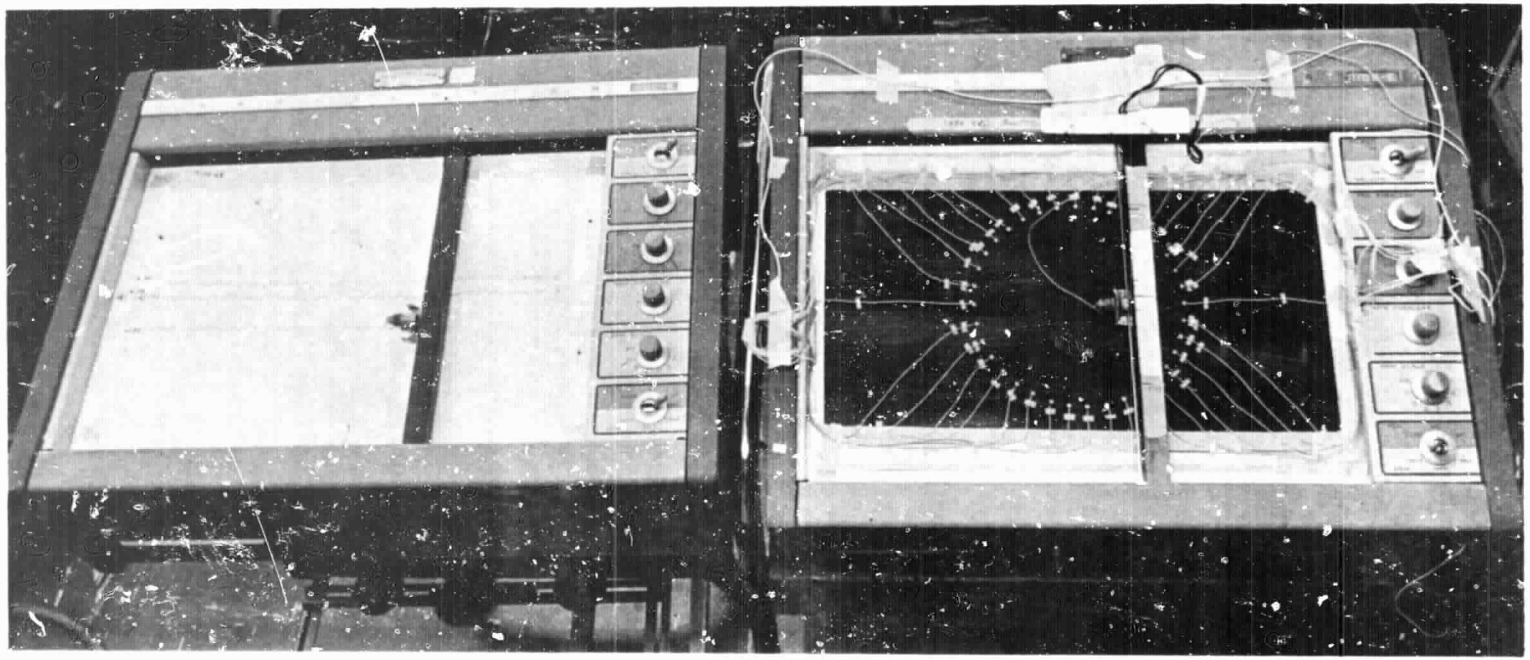

Figure 2. Close-Up of Potential Plotting of the Analog Electrical Simulation

Next aluminum foil was wrapped around the cage and grounded to one side of the sinusoidal voltage generator. The electric field at the probe dropped almost to zero. Leakage through the top and bottom of the cage resulted in a small residue of field.

Then all the wires of the cage were electrically shorted by a conducting wire. Again the field at the probe reduced to the leakage field level. This demonstrated that the arrangement of wires provided as good a Faraday cage as an aluminum sheet wrapped around the cage.

F. SWITCHING OF THE FARADAY CAGE

After determining the arrangement of wires necessary to provide adequate field chopping action, it was necessary to decide upon the method of switching the cage from an open to a closed position at rates as high as 1000 Hertz.

The final design of the cage uses 96 wires; these wires must be alternately shorted and opened. The technique chosen to switch the cage mode uses the plasma of the ionosphere as part of the switching circuit.

Each wire is terminated with an IN4148 diode; the wires are alternately connected to the base and collector of the diodes. Thus a series path from the switch actuator (±5 volt square wave generator) through 48 diodes in parallel connected to alternate wires, through the plasma between the wires, then through the next 48 diodes again in parallel and back to the square wave generator.

The technique was to test two dimensionally, again using resistance paper and silver paint. A field probe in the center of the cage configuration measured the electric field when the cage was opened and closed. Figure 3 shows the arrangement. The diodes were switched at 400 and 4000 Hertz and for square wave voltages between ± 2 to ± 5 volts. The same amount of shielding and penetration of the electric field was obtained as when the wires were physically opened and shorted.

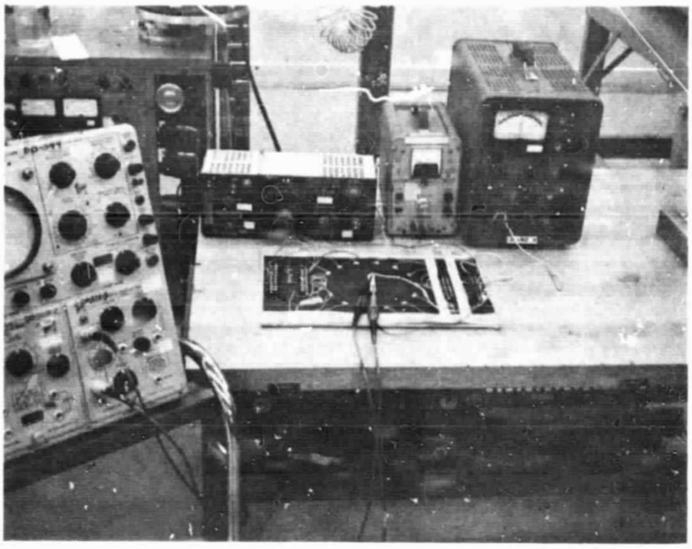

a) Experimental Set-Up

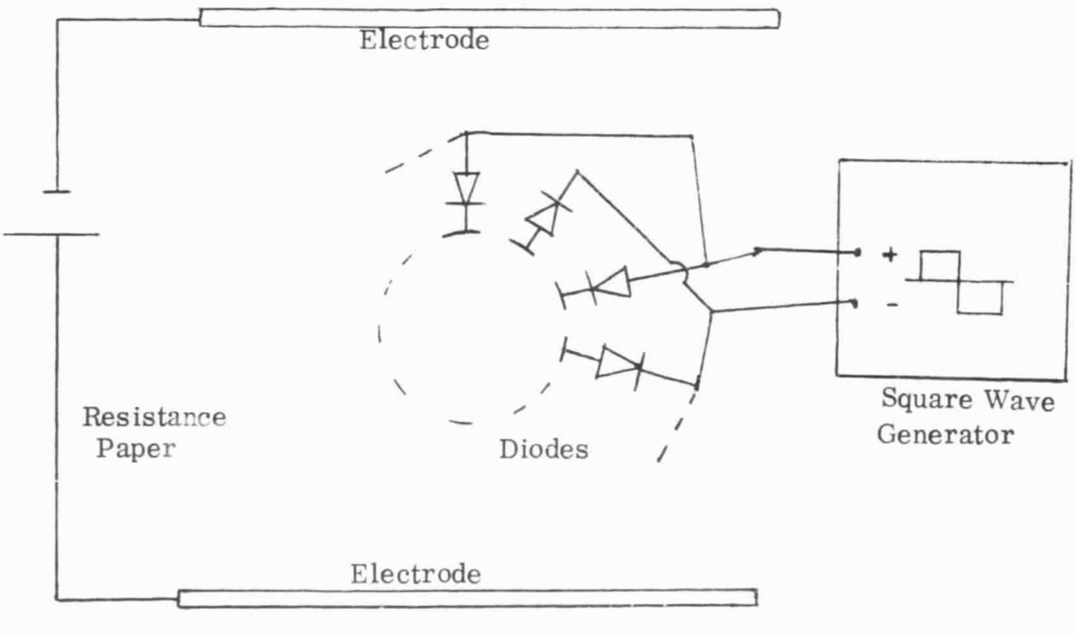

b) Schematic

Figure 3a & b. Diode Switching Configuration (Analog)

G. DESIGN OF FARADAY CAGE

Based upon the analysis and the anlog computer results, a system of thin wires arranged concentrically around the beam was chosen. The analysis demonstrated that for adequate reduction of distortion, the wires should be arranged symmetrical and in groups of fours. Further, for adequate field cancellation the number of wires should be large. The measure of largeness and the influence of wire geometry and positioning were explored experimentally using the analog computer. The result of this investigation resulted in an arrangement of wires in two concentric circles about the electron beam. The total number of wires is 96, where 48 wires are located on an eight inch diamter circle and the rest on a nine inch diameter circle. The wires in each row are about one-half inch apart and the rows are interlaced so that each wire on the inner circle is midway between the wires of the outer circle. The diameter of the wire originally chosen was 32 mils, however in fabrication it was found that 20 mil wire was better. Since it was desirous to use as thin a wire as possible to reduce the extent of the plasma sheath penetration into the Faraday cage, the thinner wire was used. Theoretically, electric fields produced by the plasma sheath around the wires should decay as a strong function of (R/λ_D), where R is the ratio of distance between the wire and the electron beam to the radius of the wire, and λ_D is the Debye length of the ionosphere. Typically this electric field is negligible 100 body radii from the wire. Figures 4a and b show the electric field meter.

H. MECHANICAL CAGE

The problems associated with an electrical cage operating within the ionosphere are numerous, as this investigation has indicated. An obvious alternate approach is a mechanical cage which closes and opens by mechanical means at some set rate. The variation of the magnetic field strength is a function of satellite position, makes it desirous to have as fast a chopping rate as possible. However, the weight and size limitations of the field meter have led the preliminary design considerations to limit the rate to below 10 cycles per second. One of the

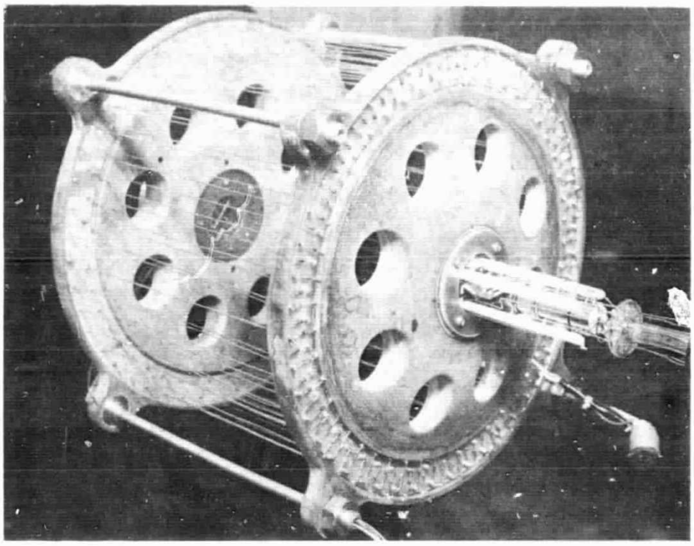

a) Electron Gun and Diode End

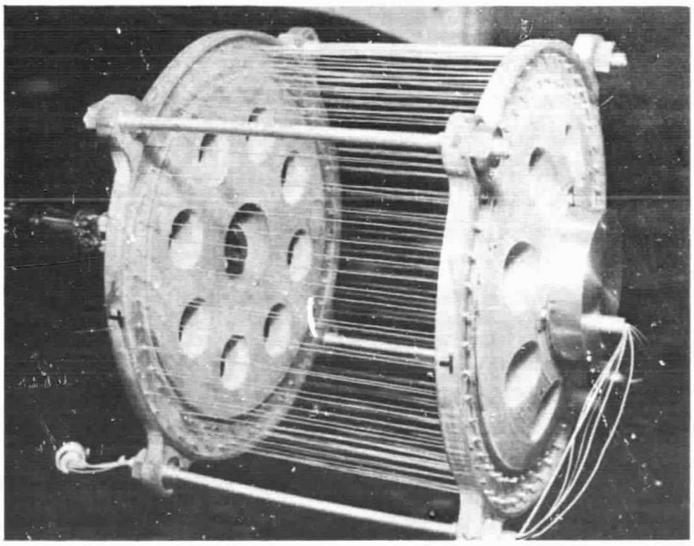

b) Target and Amplifier End

Figure 4. Electron Beam Electric Field Meter

designs is illustrated in Figure 5. This design minimizes the amount of cage remaining while the cage is open and the rate of chopping is twice the rotation rate to minimize vibration noise of the readout signal. This cage is completely closed twice during each rotation of the vanes, thus complete electric field elimination, regardless of the plasma parameters, occurs.

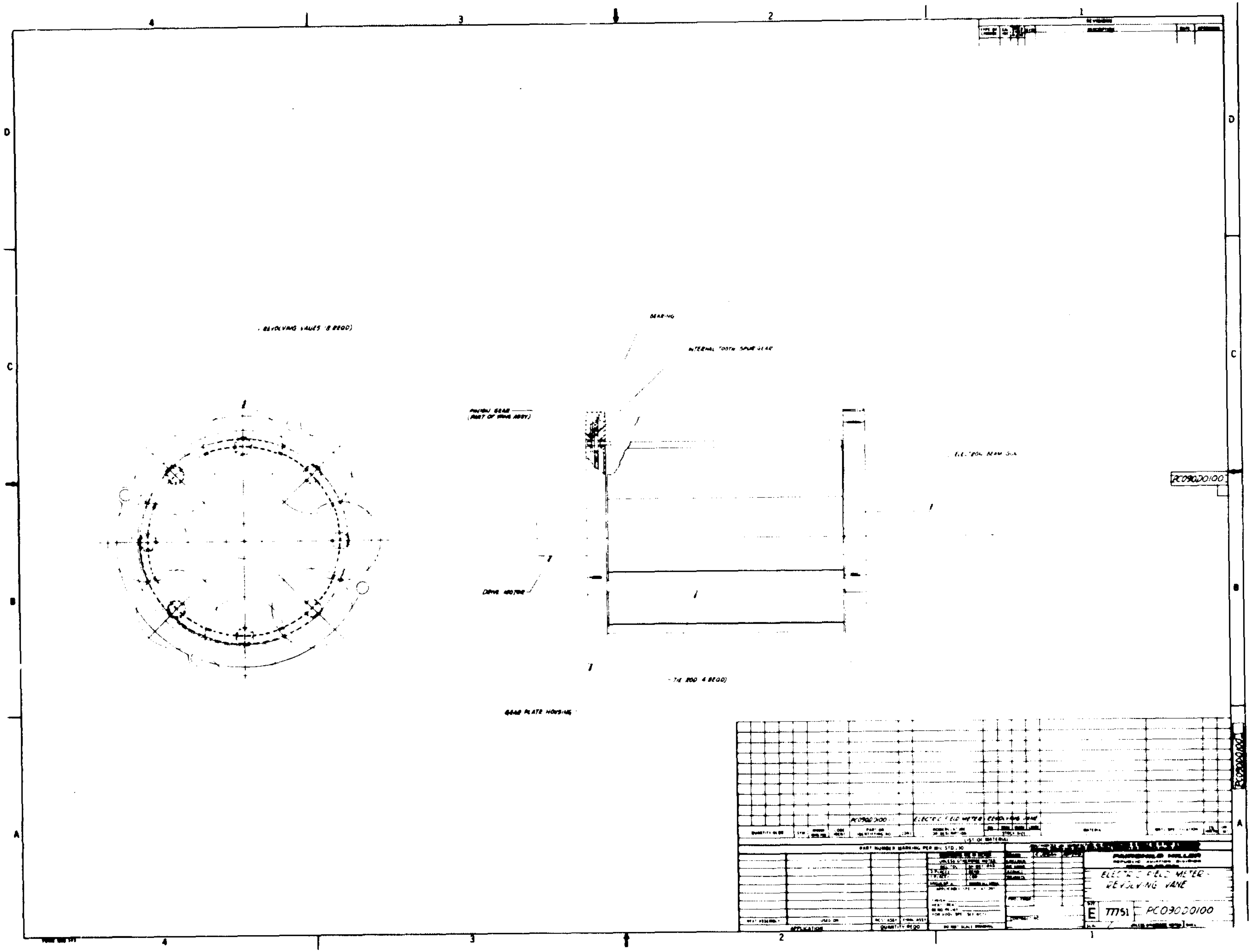

Figure 5. Mechanical Faraday Cage

SECTION III

FIELD METER OPERATION

A brief description of the electric field meter design concept is presented herein; more details are to be found in Reference 9.

There are two major difficulties in measuring ionospheric electric fields by deflection of an electron beam. The first is that the ambient electric field deflection is very small. The second is that the Earth's magnetic field introduces a ver large deflection. For a 500 volt beam, a magnetic field of 1 gamma produces as much deflection as an electric field of 14 millivolts/meter. Since the Earth's field can be of the order of 40, 000 gamma, a signal to noise ratio of 1/560, 000 must be overcome in order to resolve one millivolt/meter.

The means chosen to discriminate between the deflection due to magnetic versus electric fields is to modulate the electric field in a precise manner, by alternately creating and removing a Faraday shield around the beam. The magnetic field is unaffected by this, while the electric field is modulated in a squarewave fashion. By demodulating the output signal synchronously with the modulation, only the squarewave signal is accepted. In order to accurately measure deflections without requiring an extremely accurate mosiac target or other such device, the closed loop beam centering system is employed. A current collector target is divided into four segments. The currents collected in two opposing segments are balanced against each other. The difference signal when amplified and applied as the voltage to an appropriate pair of deflection plates is then a direct measure of the field induced beam deflection. The component of this voltage which is synchronous with the chopper represents the electric field while the steady state voltage represents the magnetic field. It should also be noted that there is virtually no requirement on drift or D.C. offset of the amplifiers in the loop, or on mechanical or thermal stability. Any misalignments in the gun target arrangement will contribute to the D.C. deflection plate voltage and will not affect the electric field reading.

Figure 6 is a functional block diagram of the meter showing some of the parameters of the loop. The conversion constants from electric and magnetic field to deflection are based on a 500 volt beam. A realistic design goal for the accuracy of this meter should be ± 1 mv/m over a range of 100 mv/m and ± 1% accuracy over a dynamic range of 100 mv/m to 1000 volts/meter. The upper limit is determined by the ± 100 volts limitation of the readout equipment and power supplies.

A. ELECTRON BEAM CHARACTERISTICS AS A FUNCTION OF PRESSURE

The electron beam utilized in the meter must traverse 0.27 meter (10.5 inches). The attenuation of the electron beam due to collisions with gas molecules was discussed in Reference 9. The spatial rate of change of beam current along its path is given by:

$$\frac{dI}{dz} = -\mu \rho I$$

$$I'/I_o = \exp(-\mu \rho z)$$

where I_o is the initial beam current

I' is the beam current at the target.

The logarithmic decrement of beam current (μ) for nitrogen at 600 volt acceleration voltage is 1.24×10^7 cm^2/gm. The gas density at 10^{-3} Torr is 2×10^{-1} gm/cc. Thus the percentage of beam reaching the target should be about 50%, and reducing to less than 1% at 10^{-2} Torr. The beam current was monitored from 10^{-5} Torr up to 10^{-2} Torr. The actual current collected by the target is shown in Table II.

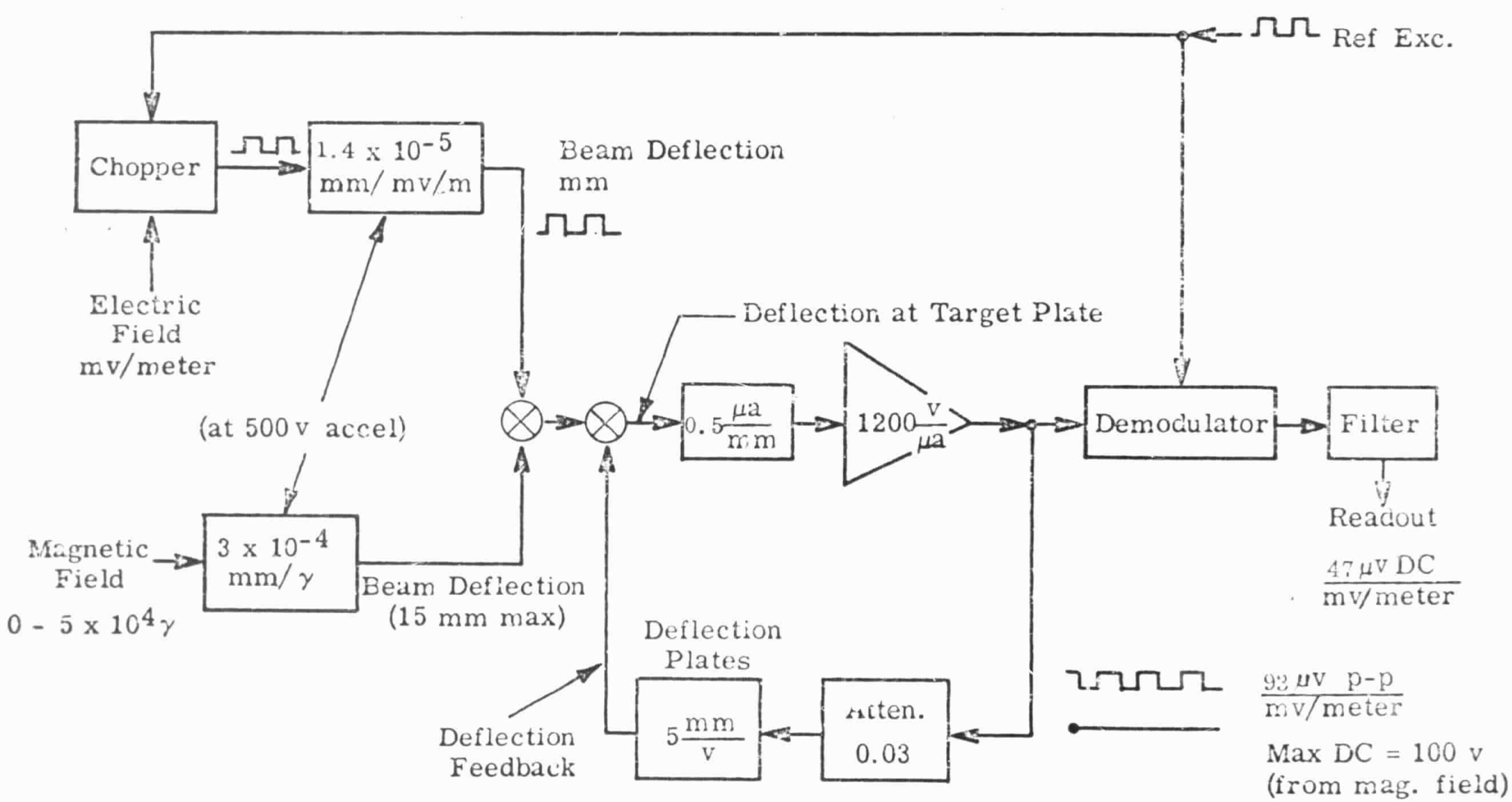

Figure 6 : Electric Field Meter System - Block Diagram (Single Axis Shown)

Table II. Current Collected at Target vs. Pressure

Pressure (Torr)	Beam Current at Target (Microampere)
10^{-5}	1.6
10^{-4}	1.4
10^{-3}	0.5
2×10^{-3}	0.3
5×10^{-3}	0.1
10^{-2}	0.05

B. OPEN LOOP OPERATION

The electric field meter was placed within a bell jar for calibration, nitrogen gas was allowed to enter through a controlled leak raising the pressure from 10^{-5} to 1.5×10^{-2} Torr. As the pressure rose, signals to both the x and y preamplifier and the output of the final amplifiers were monitored. The forward gain of both A.C. and D.C. signal are shown in Table III.

Table III. Forward Gain as Function of Pressure

Pressure (Torr)	D.C. Gain		A.C. Gain	
	x	y	x	y
10^{-3}	1000	100	540	100
5×10^{-4}	850	100	540	100
10^{-3}	750	75	500	100
2.5×10^{-3}	200	75	400	100
6.5×10^{-3} (raised filament power)	600	280	600	400
1.5×10^{-2} (changed A_3 gain setting)	1200	200	650	250

Since the closed loop system gain is $K/(1+\beta K)$; where K is the forward gain and β is the feedback, when K is 100 or more and β is about 0.1 or more, then this can be approximated by $1/\beta$. We found that by adjustment of amplifier gain and filament power, the forward gain can be in the order of 100 or better for both axis from 10^{-5} to 1.5×10^{-2} Torr pressure range.

C. CLOSED LOOP OPERATION

After assuring that sufficient forward gain was possible over a pressure range from 10^{-5} to 10^{-2} Torr, the loop was closed by applying a feedback voltage on the deflection plates of the electron gun. Since when the loop is closed all D.C. level shifts are removed, only the A.C. gain between the preamplifier to the output was monitored. The A.C. gain as a function of pressure with a stable closed loop operation is shown in Table IV.

Table IV. Closed Loop Gain as Function of Pressure

Pressure (Torr)	Closed Loop x	Forward Gain y
5×10^{-5}	230	350
10^{-4}	200	280
10^{-3}	200	280
5×10^{-3}	200	200
10^{-2}	100	100

D. SCALE FACTOR CALIBRATION

Since the amount of beam current per millimeter of deflection change and the deflection per volt applied to the deflection plates are part of the closed loop, the calibration of the meter is accomplished by establishing the loop electronic parameters then observing the output voltage as a function of applied field.

For an applied field of 60 volts/meter, the outputs of the final amplifiers (A_3 in both x and y) were 2.6 volts. Thus the scale factor at a pressure of 5×10^{-3} Torr was 46 millivolts per volt per meter. The scale factor was checked at 120 volts/meter. These electric field values were used in the calibration because typical fields in the positive column of the glow discharge are quite high.

E. CLOSED LOOP PERFORMANCE WITHIN THE IONIZED CHAMBER

The assembled electron beam electric field meter was placed within the glow discharge chamber. The chamber was evacuated to 10^{-6} Torr, then nitrogen was introduced through a controlled leak to raise the chamber pressure to the glow discharge ignition point. Glow discharge and closed loop operation occurred from pressures slightly less than 10^{-3} Torr up to 8×10^{-3} Torr. Above this pressure, the loops tended to oscillate, while below 10^{-3} Torr the glow could not be ignited.

At 5×10^{-3} Torr in nitrogen, the loop parameters were established. Based upon the bell jar calibration, the output of the loops were 46 millivolt per volt/meter. This output was filtered and the voltage read on an A.C. differential Fluke voltmeter. The attenuation of signal due to filtering was 0.42. Thus for each volt of measured output on the Fluke voltmeter, the field has a strength of 52 volts/meter.

The diodes were triggered by a squarewave generator at 1 kHz and 10 kHz; the discharge voltage was varied from 1100 to 1660 volts and the discharge current varied from 1 m amp to 6 milliampere. The average electric field value on the X axis was about 52 volts/meter and on the Y axis 26 volts/meter, at the higher discharge currents (3 m amp - 6 milliampere), there was close agreement between the 1 kHz and 10kHz chopping rates. However, the results of these measurements are questionable. The reasons for the doubts are discussed in Section IV of this report, where the action of the cage as a function of pressures using an electrostatic probe are discussed.

SECTION IV

FARADAY CAGE OPERATION IN PLASMA ENVIRONMENT

A. PLASMA FACILITY

A large glow discharge tube was constructed to test the electric field meter. The diameter of the discharge tube was dictated by the requirement that the mean free path be larger than the meter, while smaller than the tube diameter. This feature minimizes wall effects.

The tube is made of six sections of 2-foot diameter glass pipe. These sections are mounted on carriages and ride on the rails of a main frame. This allows for a maximum electrode separation of 14 feet. The ends of the sections have a flat ground face which seals against a teflon gasket.

The electrodes are aluminum discs whose diameter is slightly smaller than the tube diameter. To eliminate some of the electrical noise from the discharge pointed steel pins were inserted into the cathode to achieve brush cathode action. It is known that cold cathode discharges that use a brush cathode are electrically much quieter than the conventional cold cathode discharge.

The vacuum system for the tube consists of a roughing pump and a 4-inch pumping station.

The lowest pressure that we can achieve under normal operating conditions is 10^{-6} Torr. The measured leak rate is less than 10^{-3} Torr per hour.

The power supply for the tube is 3,500 volt, 2 ampere supply. The long length of the tube allows us to stay on a part of the Paschen curve such that the necessity for a starting circuit is eliminated. A variable resistor bank is used to adjust the load line to the desired operating point. Figures 7 and 8 are photographs of the apparatus.

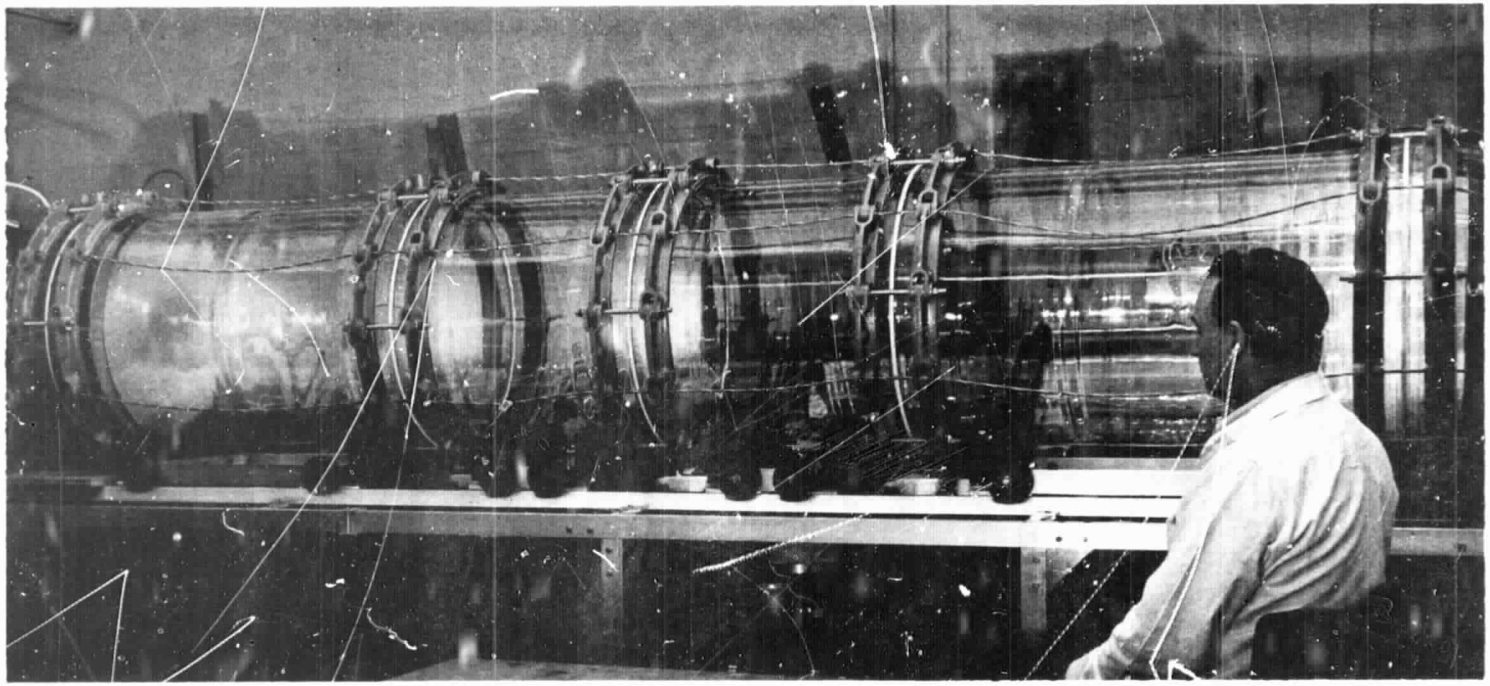

Figure 7. Low Pressure Glow Discharge

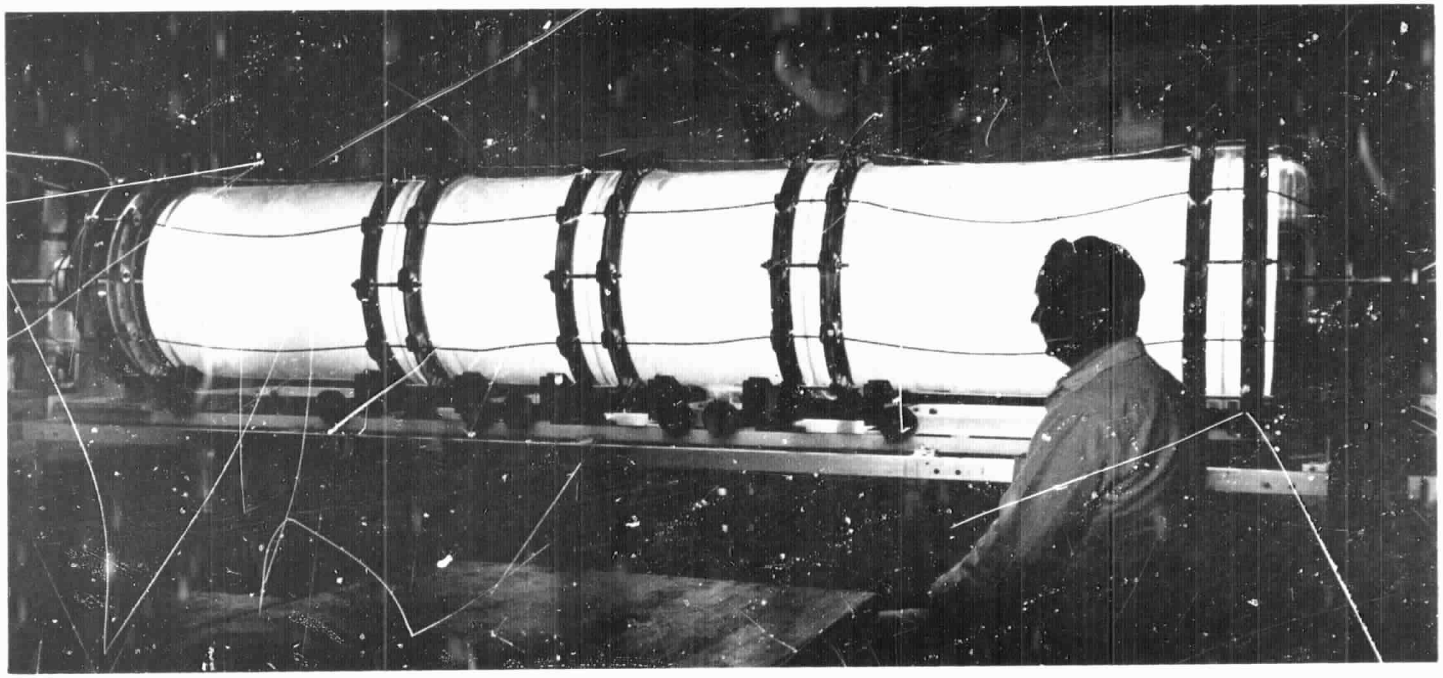

Figure 8. High Pressure Glow Discharge

B. EXPERIMENTAL RESULTS

A double Langmuir probe was used to measure plasma density and electron temperature. Measurements of these plasma parameters have been made in one plane of the tube. Figures 9, 10, and 11 are measured probe characteristics. Table V is a list of the reduced probe data. The density was determined by using a simplified ion current saturation formula:

$$I_p = \frac{1}{2e} A_p \eta_o \left(\frac{k T_e}{M}\right)^{1/2}$$

where:

I_p = ion saturation current

e = electronic charge

A_p = probe area

T_e = electron temperature

M = mass of the ion

η_o = electron density

P	η_o ($\frac{\text{electron}}{\text{cm}^3}$)	T_e (^{o}K)
375 μ	4×10^7	1.7×10^4
100 μ	5×10^7	$.8 \times 10^4$
50 μ	4×10^7	2.2×10^4
10 μ	2×10^8	$.55 \times 10^4$
5 μ	8×10^7	1.9×10^4

Table V.

This equation overestimates the density because it ignores sheath effects which increase the effective current collecting area of the probe. It will, however, determine the electron density correctly to an order of magnitude. The probe data was analyzed by the two tangent method. Figure 12 is a schematic of the probe measuring circuit.

The probes were driven by a variable voltage source which swings the probes plus and minus. The source consisted of a series battery and a voltage divider. The probe current was measured with a Fluke isolation amplifier, model A88. This amplifier has an impedance that is greater than 5×10^{11} ohms between input and output. Fluke Digital Volt Meters were used to measure probe voltage

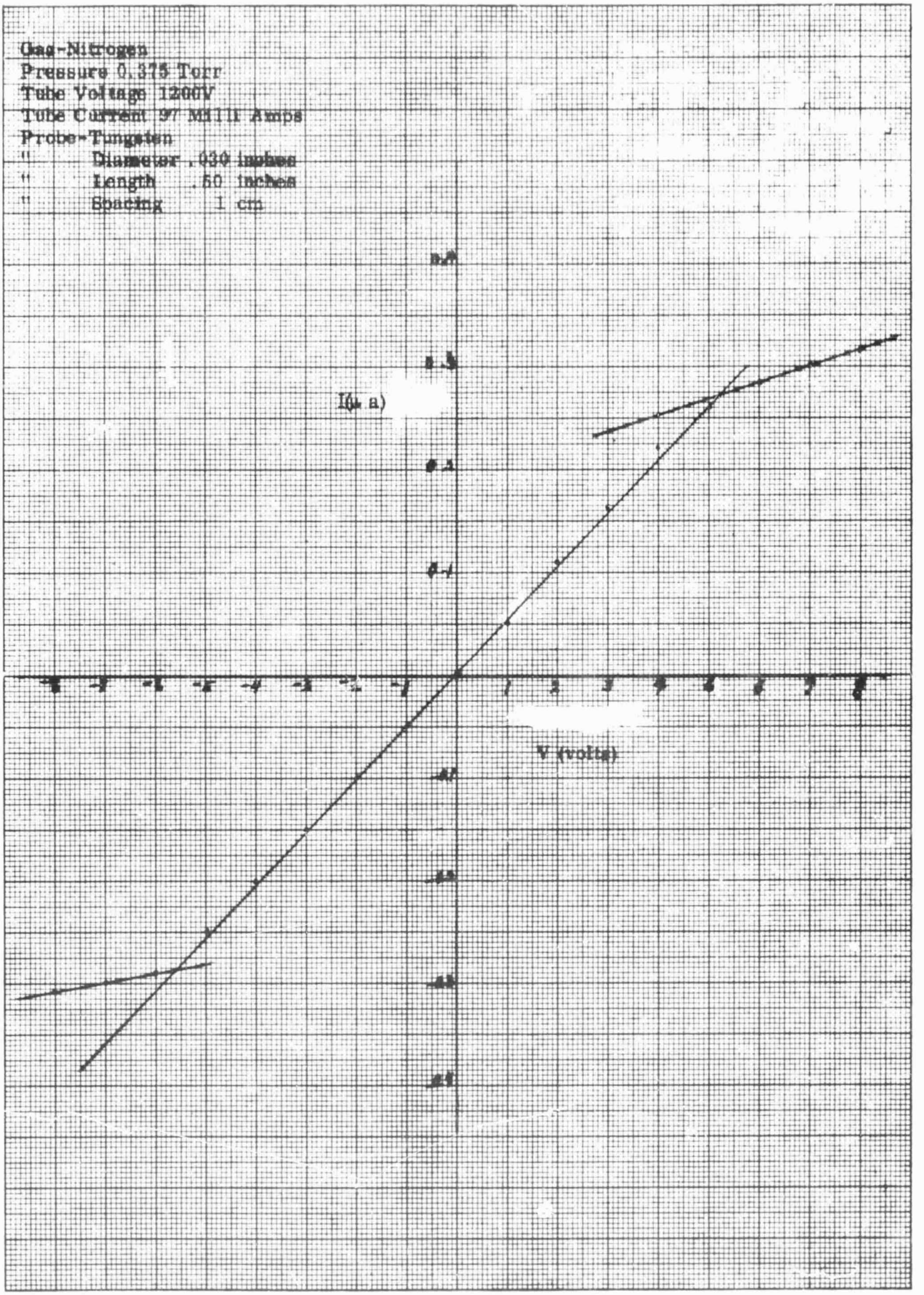

Figure 9. Probe Characteristics (High Pressure)

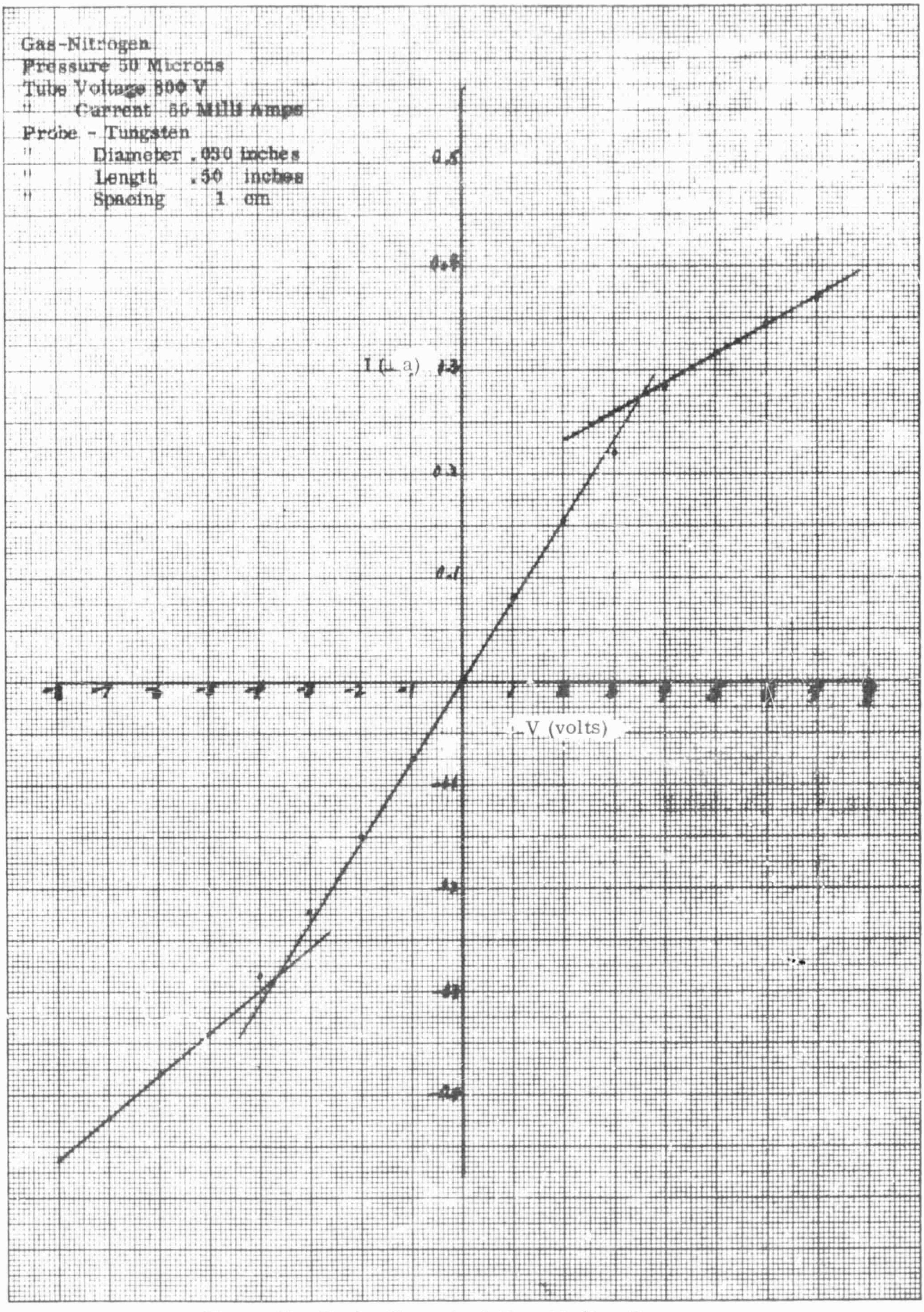

Figure 10. Probe Characteristics (Medium Pressure)

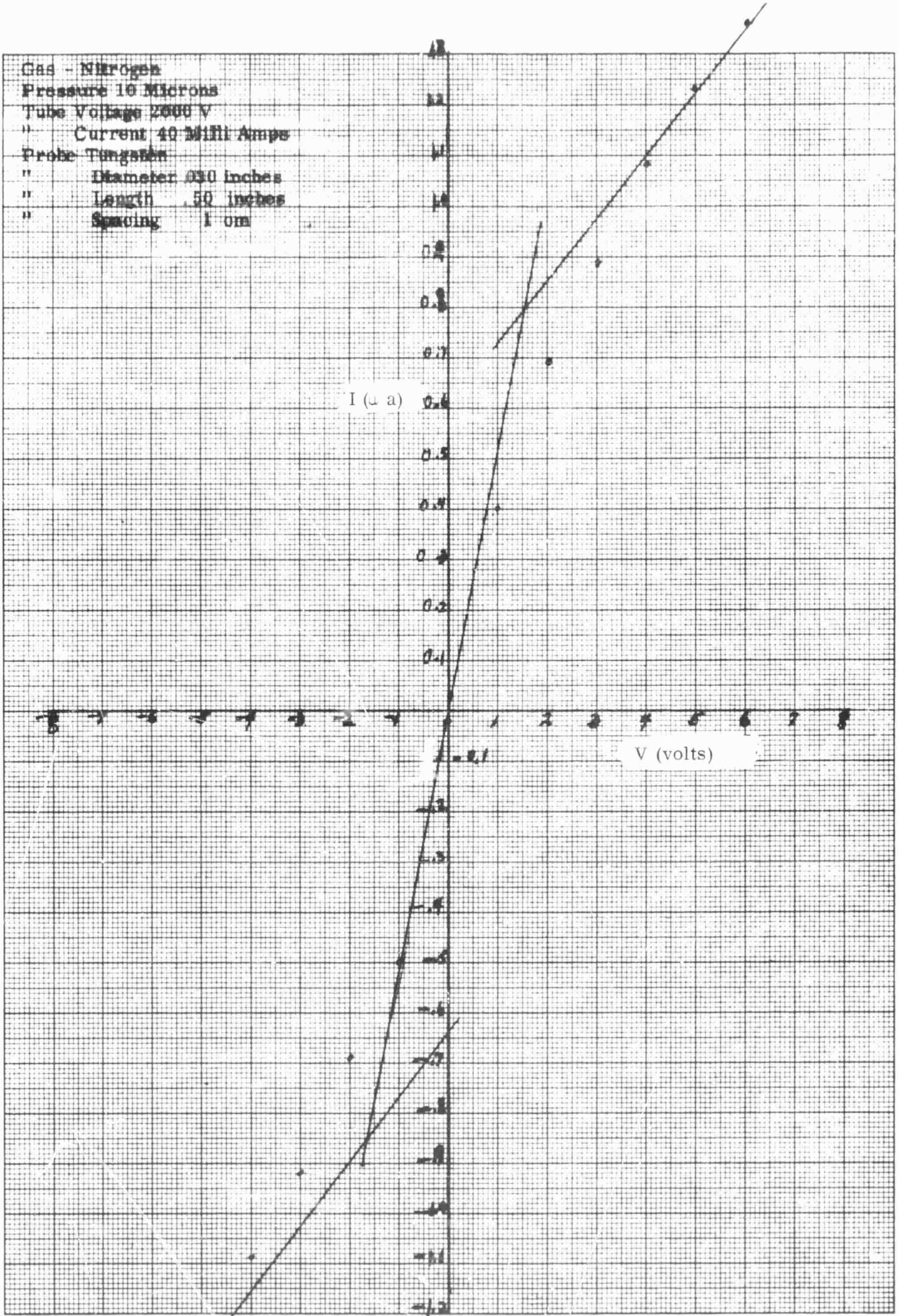

Figure 11. Probe Characteristics (Low Pressure)

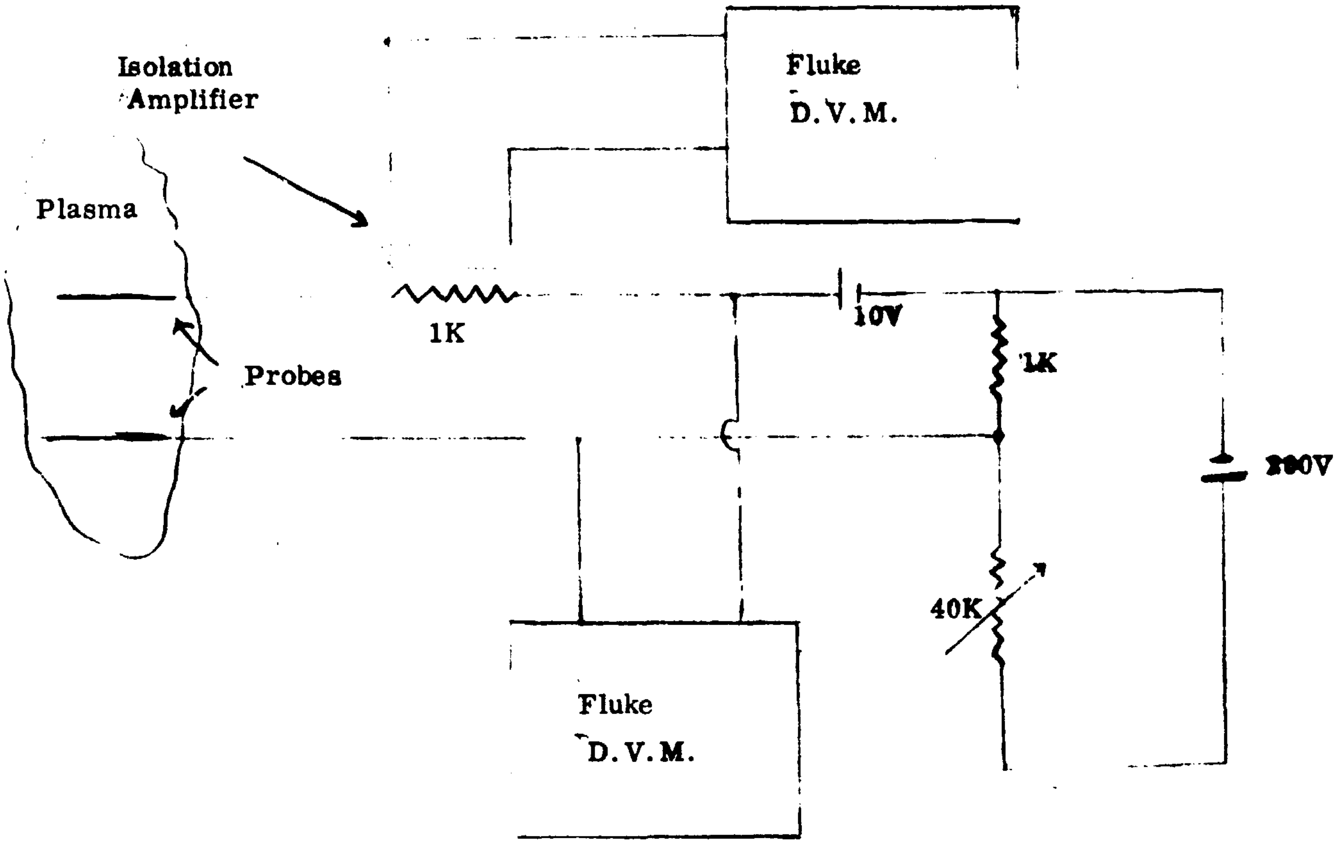

Figure 12. Double Probe Measuring Circuit

and probe currents. The Fluke D.V.M's were isolated from the line voltage with an isolation transformer. The isolation between the D.V.M's and the discharge ground was greater than 10^9 ohms as measured by an insulation tester.

The electric field in the discharge is measured by turning the double probe so that it was in line with the discharge. The probe is driven to the zero current condition. At this point the probes are floating. If we assume that both probes have equal floating potentials then the external driving voltage measures the electric field in the discharge. Table VI shows the electric field as a function of discharge parameters. The electric field measurement was checked by running the discharge at a pressure of 500 microns in nitrogen. The discharge was operated as a normal glow discharge. The measured electric field was 3.25volts/ cm. This is in agreement with the literature for large values of pR[10].

Electric Field (V/cm)	Pressure (Microns)	Tube Voltage (Volts)	Tube Current (Milliamps)
5.19	450	1800	90
4.2 1	300	1700	90
3.91	200	1400	90
2.50	100	1850	55
1.20	50	800	20
.650	10	1250	20
.420	5	1700	20

Table VI. Table of Electric Field Values

Next, the Faraday cage was positioned over the Langmuir probe. The probe was then in the center of the cage and directed along the cage axis, Figure 13. At a pressure above 110 microns the cage was always closed. This was evidenced by the probe response. The probe was driven more than 10 volts plus and minus. No probe current was registered indicating no plasma in the cage. The probe was then oriented along the discharge tube axis, and driven to the zero current conditions. Again, no field was observed. At pressures below 100 microns the cage was always open. This was evidenced by good probe response. Figures 14, 15, 16.

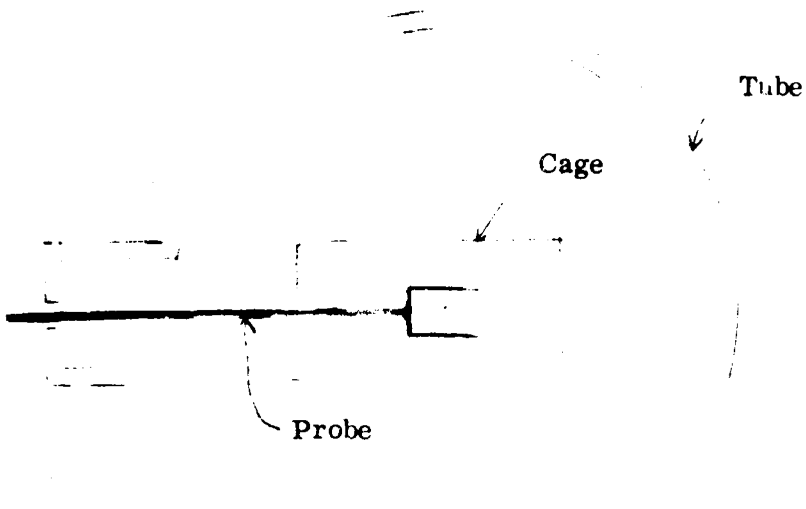

Figure 13. Probe Orientation in the Faraday Cage

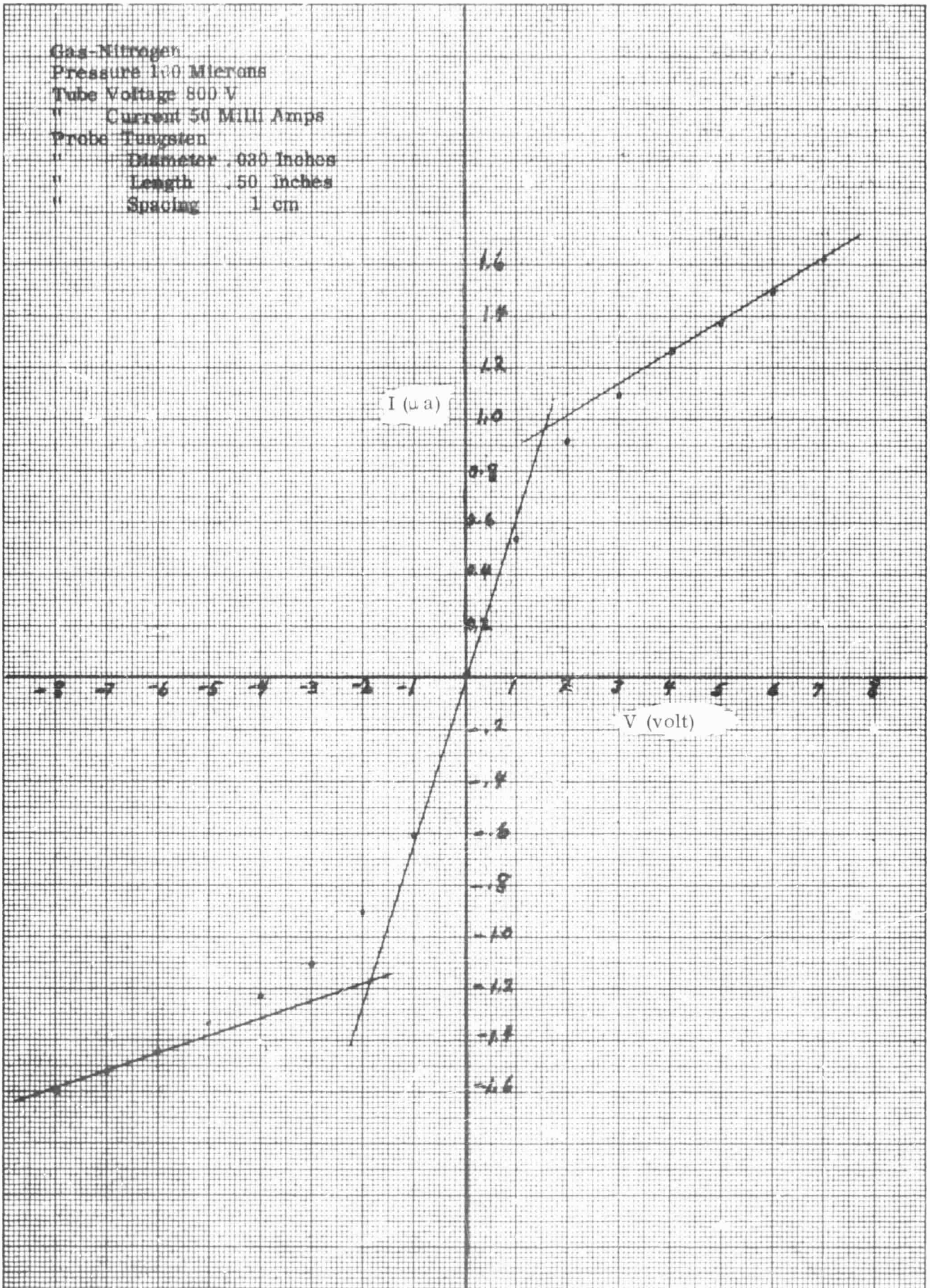

Figure 14. Probe Characteristics with Cage Over the Probe.
(Pressure - 0.1 Torr)

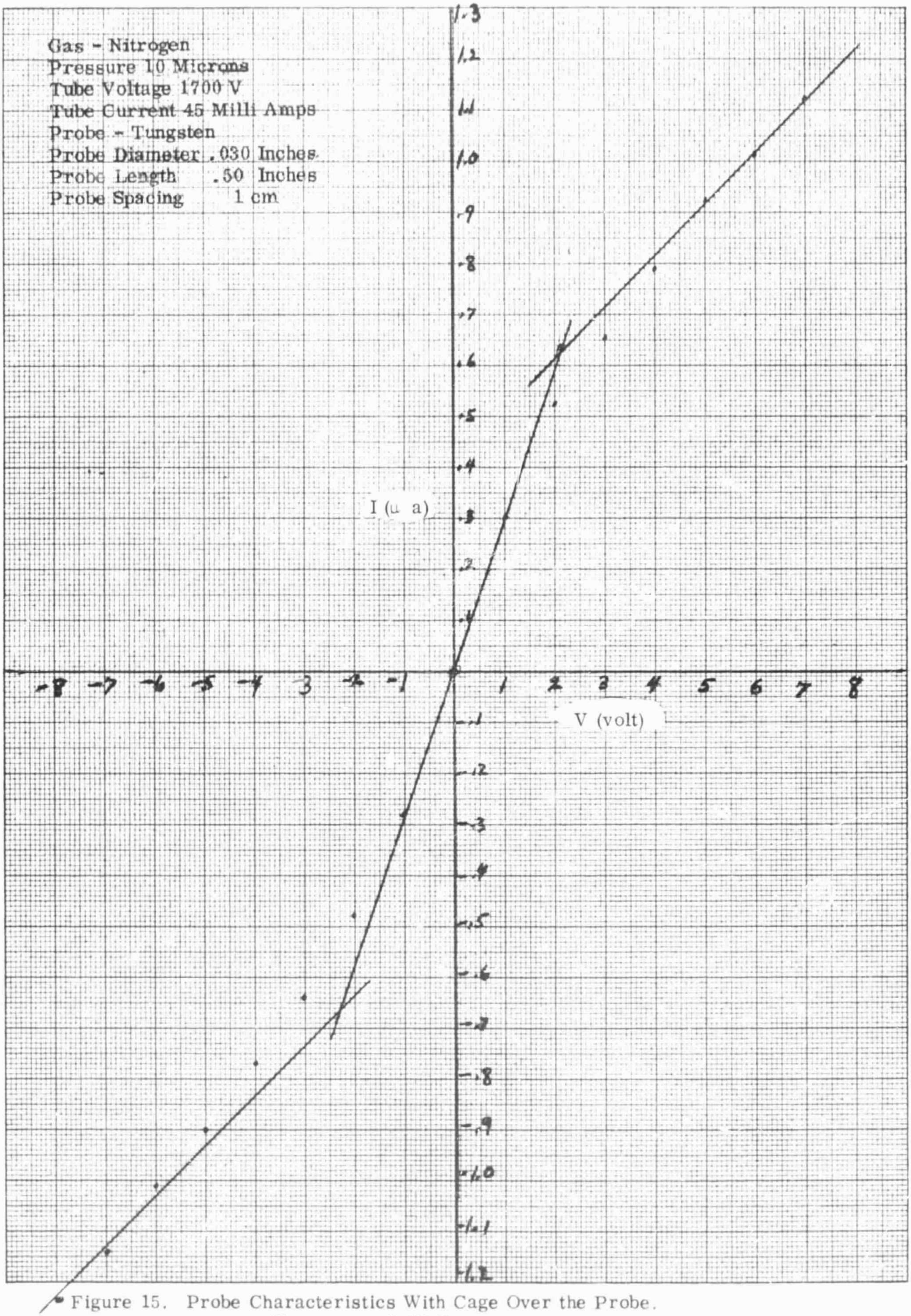

Figure 15. Probe Characteristics With Cage Over the Probe.
(Pressure - 0. 01 Torr)

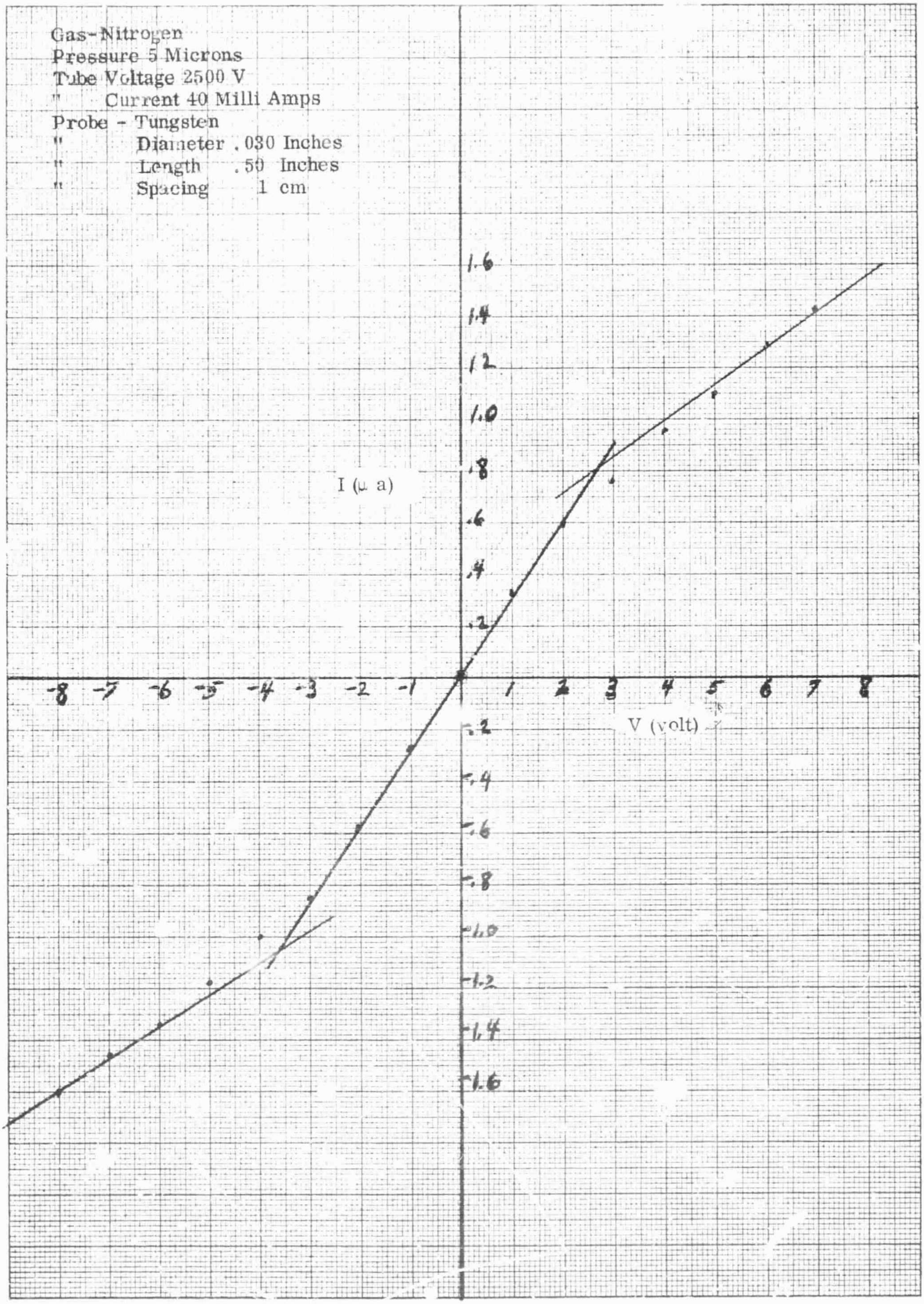

Figure 16. Probe Characteristics With Cage Over the Probe.
(Pressure - 0.005 Torr)

Table VII is the reduced probe data with the cage open. These measurements were made with the diodes both open and closed. Stated more directly, the diodes had no effect. A different approach was then tried. An auxiliary electrode was placed into the discharge tube, between the anode and the cage. This electrode was made of metallic honeycomb. It was placed in a plane parallel to the electrodes. Figure 17 is a schematic of the arrangement. In this arrangement the auxiliary electrode is connected directly to one wire of the cage. At pressures from 200 microns down to 110 microns the cage remained closed unless the diodes were activated by an external 3 volt battery. When the diodes were activated, this connected all the cage wires together, and the cage was open. This was determined by probe measurements along the discharge axis and perpendicular to the axis. The Faraday cage could be opened and closed by activation of the diodes to 110 microns. At this pressure the visible sheath structure around the cage changed as if we had switched the diodes on. Below 110 microns the cage always remained open. Figure 18 shows the electrical connections to the cage, and the auxiliary electrode.

Pressure (Microns)	$n\ (\frac{\text{electrons}}{\text{cm}^3})$	$T_e\ {}^{\circ}K$ (electron temp)
100	2×10^7	$.7 \times 10^4$
10	3×10^7	$.4 \times 10^4$
5	10^8	1.9×10^4

Table VII. Reduced Probe Data From Langmuir Probes With Cage Over Probe

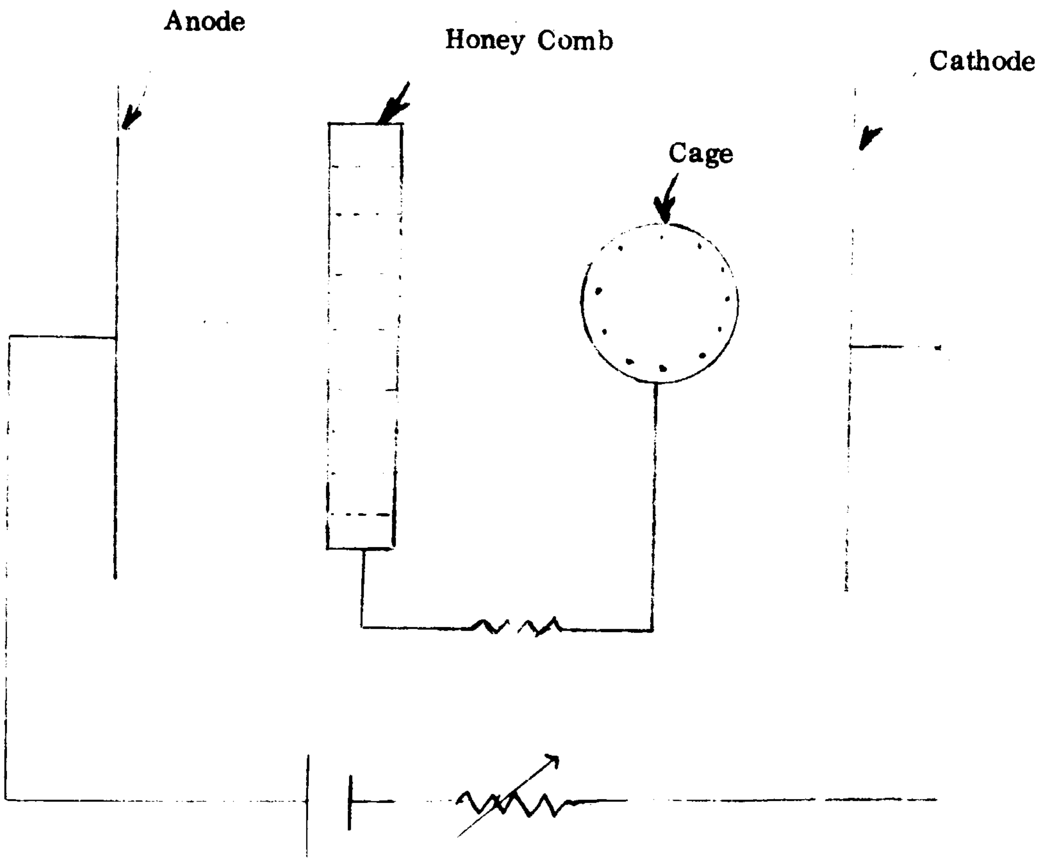

Figure 17. Auxiliary Electrode Connected to Faraday Cage.

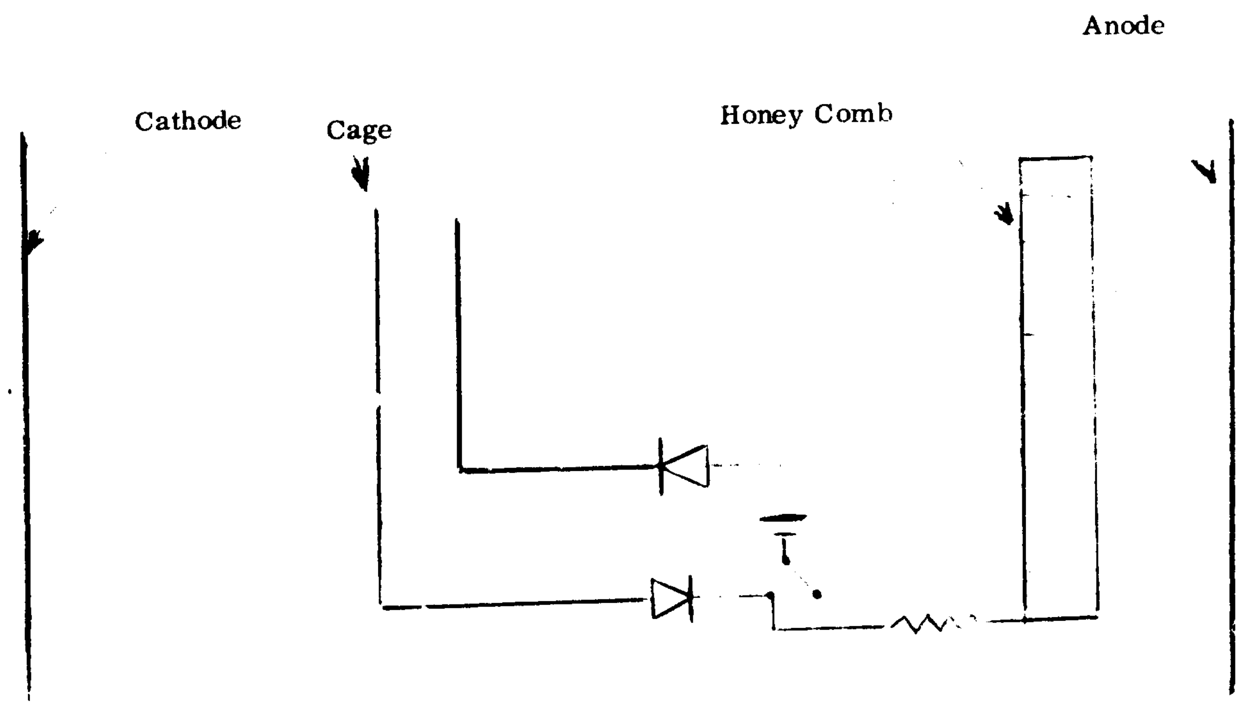

Figure 18. Electrical Connection of Cage Hone comb.

C. DISCUSSION OF RESULTS

The analysis of Section II, employed in the design of the Faraday cage, was apparently inadequate to predict operation in the plasma of the discharge tube. The most immediate explanation for this behavior is the error introduced by the linear relations between field and current involved in Laplace's equation. The more complete approach is to couple the Boltzmann equation to Poisson's equation. Immense complexities result from this approach even in simple probe theory, becoming intractable when collisions are included. When an array of probes (the Faraday cage is composed of individual wires resembling probes)is then placed in a plasma containing an external field, a complete analysis becomes a Herculean task.

However, some understanding of the results may be attained from probe theory. One characteristic is the saturation of the ion current to the probe. Another is the equality of the ion and electron current at the probe surface. In a plasma, the electric field is inseparable from the current. For a conducting shield such as the cage to produce a region of zero electric field, the conductors and the plasma around them must carry the current which would otherwise flow in the shielded region. Since this current is limited by the saturation characteristics the shielding properties are also limited.

Another approach to Faraday cage operation in a plasma is to take advantage of the sheath which forms about a probe. When the sheath is of small thickness compared to the wire diameter, the total current to the wire is given approximately by the particle flux times the probe area. Thus, in the limit of small sheath thickness, the total current to the wires is proportional to the number of wires times the diameter of a single wire. This can be quite small compared to the current through the total projected area of the outside limits of the cage. On the other hand, if the sheath thickness is large compared to the wire diameter, the effective diameter of the probe, in terms of its current collecting properties, is of the order of the sheath diameter. Thus, if the spacing of the wires is less than the sheath thickness,all of the current should be collected on the probes (Faraday cage) resulting in shielding of the interior region.

Now it is known that by biasing the probe relative to an electrode or to ground, the effective sheath diameter may be reduced in size. Hence, if one constructs a cage with fine wire size and small spacing, and the cage is floating electrically, the external field should be shielded from the interior. Now by biasing the cage, the sheath diameter can be reduced almost to zero. Then the cage should no longer provide shielding; i.e., the cage will be "open".

The above predictions are based on collisionless probe theory which is applicable when the mean free path is much larger than the sheath thickness. While the effect of collisions in probe theory has not been dealt with quantitatively, it is known that one effect of collisions is to extend the effective sheath diameter. Hence, one might expect that when collisions are significant, the cage might behave as though the sheath thickness was larger than the spacing between wires; even though the collisionless theory predicted a much smaller sheath thickness.

With the above remarks in mind, it becomes possible to interpret the data of IV B. The number density and electron temperature do not vary greatly within the range of pressures over which the data was obtained. Consequently, the Debye length remains relatively constant. In the region of large mean free path (low pressure) the Debye length is about equal to the sheath thickness and is much less than the spacing between wires. Hence, at these low pressures the cage is always open. At somewhat higher pressures, the effect of collisions serves to extend the sheath until the cage is closed. When the cage is biased with respect to ground, the sheath thickness is reduced and the cage is opened. Finally, one reaches a region of pressure in which the effect of collisions is such as to make the bias voltage ineffective in reducing the effective sheath thickness.

We are interested primarily in the low pressure region, where collisions play no role and the sheath thickness is small compared to the present wire spacing. To close the cage it will be necessary to reduce the wire spacing to a distance less than the sheath thickness (1.5mm). To make it possible to open the cage by means of a bias voltage, the wire thickness will have to be reduced correspondingly.

SECTION V
RECOMMENDATIONS

In order to achieve the goal of a Faraday cage operable in an ambient plasma environment the following program of research is recommended:

1. Analysis, based on collisionless probe theory modified by the presence of an external field, should be developed to permit a quantitative understanding of Faraday cage operation.
2. Experimentation should be performed in the glow discharge facility with fine wires closely spaced (of the order of sheath distance as described in Section IV). Such an array will be tested at a low pressure to provide simulation of the ionosphere and also operation of the electron beam.
3. Since the difficulty of operating an electrical Faraday cage over a wide range of plasma parameters is realized, a simple mechanically operated Faraday cage should be constructed and tested in the glow discharge facility.

PRECEDING PAGE BLANK NOT FILMED.

REFERENCES

1. Gdalevich and Imyanitov, "Electric Fields in the Ionosphere Based on Data from Direct Measurements of Geophysical Rockets," NASA-TT F-315, May 1965.

2. Mozer and Bruston, "Electric Field Measurements in the Auroral Ionosphere", J. Geophysical Res., February 1967.

3. Fahleson, U.: "Theory of Electric Field Measurements in the Magnetosphere with Electric Probes", Royal Inst. of Tech., Sweden, Report 66-02, February 1966.

4. Lafferty, P.: Manned Space Flight Symposium on Gemini IV, October 1965.

5. Wildman, P.J.C.: "A Device for Measuring Electric Fields in the Presence of Ionization", J. of Atm. and Terr. Physics, Vol. 127, No.3, p.417 (1965).

6. Haser, L.: "Aurora and Airglow". Proceedings, NATO Advanced Study Institute, University of Keele, England, August 1966.

7. Warren, R.W.: "Measurement of Electric Fields as Applied to Glow Discharge", Rev. Sci. Inst., August 1955.

8. Shriver, E.L.: "Investigation of the Deflection of an Electron Beam as a Means of Measuring Electric Field Strength", MSFC, NASA TX-53435, April 1966.

9. Levy, G., Jacobs, H., and Bendor, E.: "Measurement of Electric Fields in the Ionosphere", NASA/Marshall Space Flight Center, NASA CR-61189, January 1968.

10. Francis, G.: "Handbuch Der Physik", Volume XXII, pps 119,120, 1956.

PRECEDING PAGE BLANK NOT FILMED.

APPENDIX I
BEAM PRODUCED PLASMA IN A CYLINDER

A. INTRODUCTION

We consider here the problem of determining the stationary distribution of plasma particles produced in a cylinder by collisions of an axial electron beam with neutral atoms. Impact ionization of the neutral gas produces both ions and electrons. Some of the ions will drop into the potential well that exists in the region of the beam. If the ion density is sufficient, the condition known as ion-focussing will result. In this condition the region of the beam is essentially neutral, and beam blow-up, as a result of neutral repulsion of electrons, no longer occurs. We will assume that there is an excess of ions which with the secondary electrons produced by ionization travel to the walls where recombination takes place. It will be assumed for simplicity that the region of production of the secondaries is a geometric axial line, that the secondaries have no axial component of velocity when first produced, and that the cylinder is infinitely long.

In their progress to the wall the secondaries are subject to collisions with the neutral background gas particles and to electric fields. The fields are generally of two types: These are fields with external sources and fields which result from the distribution of the particles themselves. The general treatment of all of these effects simultaneously is presently beyond our analytic capabilities. Therefore we shall separate field and collision effects. Moreover, we shall assume that collisions are infrequent, but not absent.

B. COLLISION-FREE, FIELD FREE APPROXIMATION

The Boltzmann equation which describes the stationary state of the electrons when fields are neglected is:

$$\underline{v} \cdot \nabla f = \left(\frac{\partial f}{\partial t}\right)_c + \left(\frac{\partial f}{\partial t}\right)_s \tag{B1}$$

where f is the distribution function, which is in general a function of position $\underline{r}$ and velocity $\underline{v}$ but is independent of time (stationary state). The quantities on the right $\left(\frac{\partial f}{\partial f}\right)_c$ and $\left(\frac{\partial f}{\partial t}\right)_s$ are the rates of change of the distribution function as a result of collision and the presence of the source respectively as one follows the trajectory of a particle. The source term is present only at the center. As a first approximation we consider the collisionless case outside the beam. Then,

$$\underline{v} \cdot \nabla f = 0 \tag{B2}$$

In cylindrical coordinates (r, φ, z) Equation (B2) can be written as:

$$v_r \frac{\partial f}{\partial r} + \frac{v_\varphi}{r} \frac{\partial f}{\partial \varphi} + v_z \frac{\partial f}{\partial z} = 0 \tag{B3}$$

where v_r, v_φ, v_z are the velocity components in the r, φ, z directions respectively. We neglect end effects. Then derivatives with respect to z are zero and only two space dimensions are considered. We shall for the present neglect dependence of f on v_z as well. Since azimuthal space symmetry can be assumed, f is not explicitly dependent on φ. However, f may be implicitly dependent on φ through v_r and v_φ, therefore, Equation (B3) becomes:

$$v_r \frac{\partial f}{\partial r} + \frac{v_\varphi}{r} \left[\frac{\partial f}{\partial v_\varphi} \frac{\partial v_\varphi}{\partial \varphi} + \frac{\partial f}{\partial v_r} \frac{\partial v_r}{\partial \varphi}\right] = 0 \tag{B4}$$

Next we note that:

$$\nabla \cdot \underline{v} = 0 \tag{B5}$$

since in Cartesian coordinates the spatial coordinates and the velocity coordinates are independent variables. Since the divergence is an invariant quantity, it is also true in cylindrical coordinates. Therefore,

$$\frac{1}{r}\frac{\partial}{\partial r}(r\,v_r) + \frac{1}{r}\frac{\partial v_\varphi}{\partial \varphi} = 0$$

$$\text{or}\quad \frac{\partial v_\varphi}{\partial \varphi} = -v_r \tag{B6}$$

Also $v^2 = v_r^{\ 2} + v_\varphi^{\ 2}$ is independent of spatial coordinates. Therefore,

$$\frac{\partial v^2}{\partial \varphi} = 2\,v_r\,\frac{\partial v_r}{\partial \varphi} + 2\,v_\varphi\,\frac{\partial v_\varphi}{\partial \varphi} = 0 \tag{B7}$$

Substituting for $\frac{\partial v_\varphi}{\partial \varphi}$ from Equation (B6), we obtain:

$$2\,v_r\,\frac{\partial v_r}{\partial \varphi} - 2\,v_\varphi\,v_r = 0$$

$$\text{or}\quad \frac{\partial v_r}{\partial \varphi} = v_\varphi \tag{B8}$$

Finally, Equation (B4) reduces to:

$$v_r\,\frac{\partial f}{\partial r} + \frac{v_\varphi}{r}\left[-\,v_r\,\frac{\partial f}{\partial v_\varphi} + \frac{\partial f}{\partial v_r}\,v_\varphi\right] = 0 \tag{B9}$$

By substitution it can be seen that a solution of this equation (without being concerned about normalization) is:

$$f = \frac{g\,(v^2)}{r}\,\delta\,(v_\varphi) \tag{B10}$$

Here $\delta\,(v_\varphi)$ is the Dirac-delta function.

Let us now add the source term to the right hand side of Equation (B9), it is:

$$\left(\frac{\partial f}{\partial t}\right)_s = \frac{s(v)\,\delta\,(r)}{2\,\pi\,r}\,\delta\,(v_\varphi)\,v_r\,h\,(v_r) \tag{B11}$$

The solution of Equation (B9) with a source term on the right is:

$$f = \frac{s(v)}{2\pi r} \delta (v_{\varphi}) h(r) h(v_r) \tag{B12}$$

where h(r) is the unit step function. In Equations (B11) and (B12), vs(v) is defined as the number of electrons produced per second per unit length per unit speed interval.

Since v_z is also a constant,

$$v^2 = v_\perp^{\ 2} + v_z^{\ 2}$$

is another constant. If the collision term were absent,

$$f = \frac{1}{r} \, \delta(v_\varphi) \, \delta(v_z) \, h(r) \, h(v_r) \, g(v^2) \tag{C4}$$

could be selected as a distribution function. Here it is assumed that all the particles have a zero velocity in the z direction.

We have previously shown that where the scattering cross-section is isotropic, the target particle (neutrals) are massive and slow-moving compared to the electrons, then,

$$\left(\frac{\partial f}{\partial t}\right)_{coll.} = \frac{v}{4\pi\lambda} \int_0^{\pi} \int_0^{2\pi} (f' - f) \sin\theta d\theta d\varphi \tag{C5}$$

In Equation (C5), λ is the mean free path for scattering. The prime (′) on f designates that the independent variables are considered after collision.

Let us consider

$$I = \int_0^{\pi} \int_0^{2\pi} f' \sin\theta d\theta d\varphi \tag{C6}$$

where

$$f' = \frac{1}{r} \, \delta(v_\varphi{}') \, \delta(v_z{}') \, h(r) \, h(v_r{}') \, g(v^2) \tag{C7}$$

Then,

$$I = g(v^2) \, \frac{h(r)}{r} \int_0^{\pi} \int_0^{2\pi} \delta(v_\varphi{}') \, \delta(v_z{}') \, h(v_r{}') \sin\theta d\theta d\varphi \tag{C8}$$

That is, as an approximation to $\left(\frac{\partial f}{\partial t}\right)_{coll.}$ we are substituting the no-collision distribution function in place of f and f′ in Equation (C5). Moreover $g(v^2)$ is taken outside the integral of Equation (C8) since the speed v of the electron is not altered in a collision with a neutral (to a good approximation).

For the purpose of dealing with collisions it is convenient to transfer a spherical coordinate system. Let us define a polar angle α and an azimuthal angle β such that

$$v_{\perp} = v \sin \alpha \qquad v_r = v \cos \beta \sin \alpha$$
$$v_z = v \cos \alpha \qquad v_{\varphi} = v \sin \beta \sin \alpha \tag{C9}$$

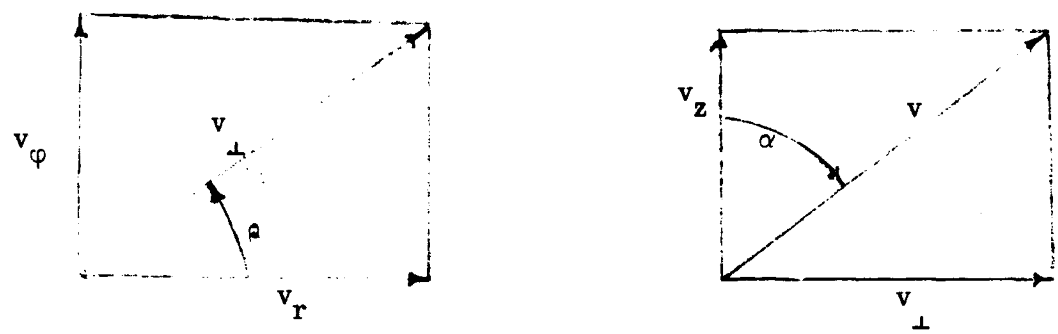

Figure 1

After collision the velocity components become

$$v_z' = v \cos \alpha'$$
$$v_r' = v \cos \beta' \sin \alpha' \tag{C10}$$
$$v_{\varphi}' = v \sin \beta' \sin \alpha'$$

In terms of Equation (C10) the integration of Equation (C8) can be written as

$$I = \frac{g(v^2)}{v^2} \frac{h(r)}{r} \int_0^{\pi} \int_0^{2\pi} \delta(\sin \beta' \sin \alpha')\, \delta(\cos \alpha') \bullet h(\cos \beta' \sin \alpha') \sin \theta d\theta d\varphi \tag{C11}$$

Let,

$$J = \int_0^{\pi} \int_0^{2\pi} \delta(\sin \beta' \sin \alpha')\, \delta(\cos \alpha')\, h\,(\cos \beta' \sin \alpha') \sin \theta d\theta d\varphi \tag{C12}$$

Now the angles α' and β' are functions of the angles α and β which give the velocity orientation before scatter and θ and φ, the scattering angles. In J the angles α and β are constants during the integration over θ and φ. Therefore,

$$J = \int_0^{\pi} \int_0^{2\pi} \frac{\delta(\varphi - \varphi_0)\, \delta(\theta - \theta_0)\, h(\cos\beta' \sin\alpha')}{\left|\frac{\partial}{\partial\varphi} (\sin\beta' \sin\alpha')\right| \left|\frac{\partial}{\partial\theta} (\cos\alpha')\right|_{\substack{\theta = \theta_0 \\ \varphi = \varphi_0}}} \sin\theta d\theta d\varphi \qquad \text{(C13)}$$

where θ_0 and φ_0 are those values of θ and φ for which $\sin\beta' \sin\alpha' = 0$ and $\cos\alpha' = 0$. Carrying out the indicated integration of Equation (C13), we obtain

$$J = \frac{N \sin\theta_0}{\left|\frac{\partial}{\partial\varphi} (\sin\beta' \sin\alpha')\right| \left|\frac{\partial}{\partial\theta} (\cos\alpha')\right|_{\substack{\theta = \theta_0 \\ \varphi = \varphi_0}}} \qquad \text{(C14)}$$

where N are number of contributions within the region $\cos\beta' \sin\alpha' \geq 0$, i.e., points where $\sin\beta' \sin\alpha' = 0$ and $\cos\alpha' = 0$. Let us refer to such points as $P\ (\theta = \theta_0,\ \varphi = \varphi_0)$.

At point P

$$\sin\beta' = 0$$

Therefore,

$$\cos\beta' = \pm 1.$$

Also, since

$$\cos\alpha' = 0,$$

$$\sin\alpha' = \pm 1.$$

But, since

$$0 \leq \alpha' \leq \pi,$$

only $\sin\alpha' = +1$ is permitted.

Also, since:

$$\cos \beta' \sin \alpha' \geq 0$$

then only

$$\cos \beta' = +1 \text{ is permitted.}$$

To summarize, at point P

$$\begin{aligned} \sin \beta' &= 0 \\ \cos \beta' &= 1 \\ \cos \alpha' &= 0 \\ \sin \alpha' &= 1 \end{aligned} \qquad \text{(C15)}$$

It remains now to find the derivatives in the denominator of Equation (C14). To do this it will be necessary to use the Law of Cosines in spherical trigonometry in which the "sides" of the spherical triangles are measured in size of the central angles of the sphere subtended. We refer now to Figure 2.

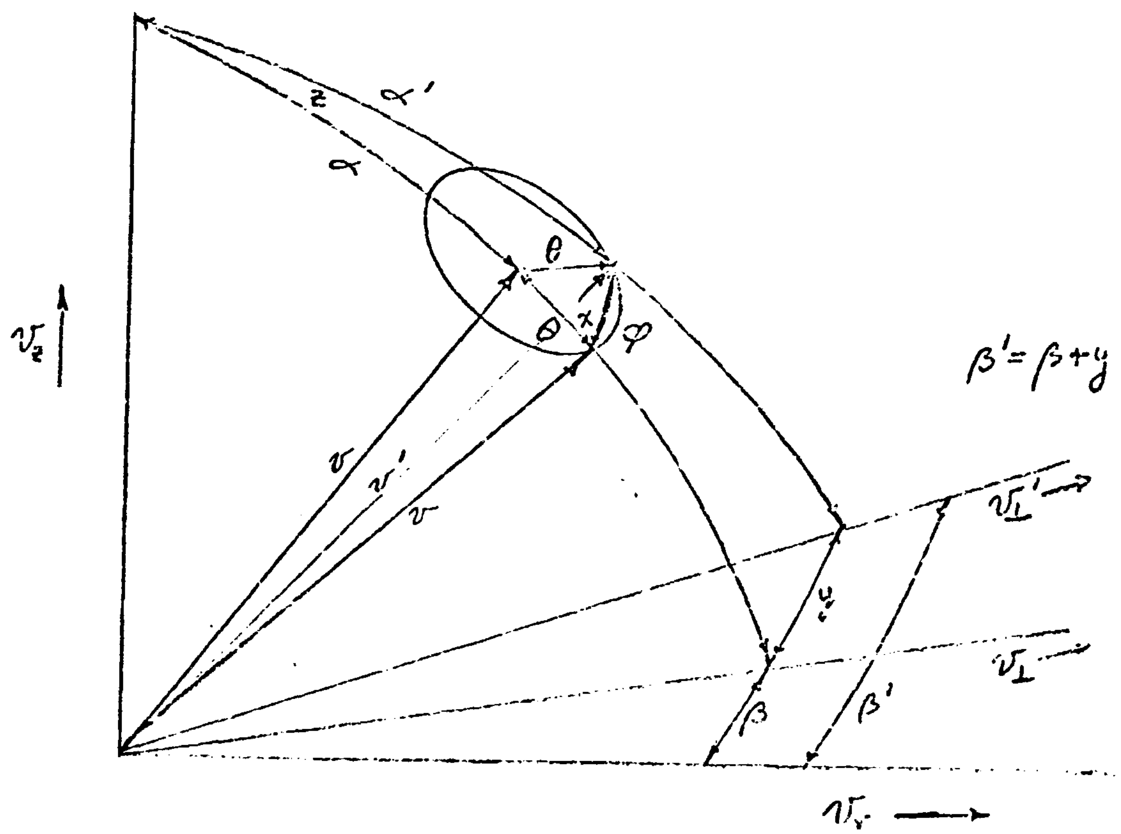

Figure 2

The sphere referred to here is the sphere whose radius is v and whose center is the point of collision. This sphere is intersected by a circular cone whose half vertex angle is θ and whose axis lies on v. The intersection of the sphere and the cone is a circle. The intersections of this circle with the $v_z v$ plane and the $v_z v'$ plane determine angle α' and φ. The angle φ must be related to a central angle of the sphere. This is shown in Figure 3.

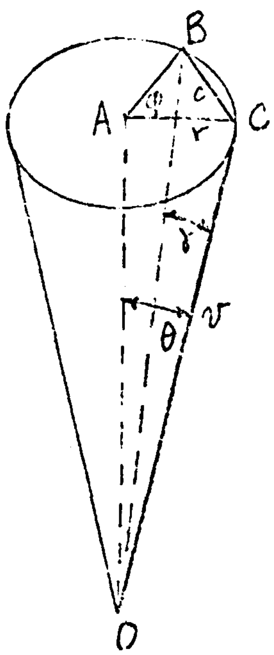

Figure 3

Consider a cone of half vertex angle θ with an angle φ swept out along the circumference of the base. The center of the base is A and the arc is BC. The chord of this arc is c and the radius of the base is r. It is desired to find the central angle subtended by the chord c. This angle is γ, and the length of the generator from vertex to base is v. Application of the Law of Cosines of plane trigonometry to triangle ABC yields

$$c^2 = 2r^2 (1 - \cos \varphi) \tag{C16}$$

In triangle OAC,

$$r = v \sin \theta \tag{C17}$$

Therefore,

$$c^2 = 2v^2 \sin^2 \theta (1 - \cos \varphi) \tag{C18}$$

Application of the Law of Cosines to triangle OBC yields

$$c^2 = 2v^2 (1 - \cos \gamma) \tag{C19}$$

If we equate the expressions for c^2 from Equations (C18) and (C19) and solve for $\cos \gamma$,

$$\cos \gamma = 1 - \sin^2 \theta (1 - \cos \varphi) \tag{C20}$$

Now we shall apply the Law of Cosines of spherical trigonometry to the angles of Figure 2. First,

$$\cos x = \frac{\cos \theta - \cos \theta \cos \gamma}{\sin \theta \sin \gamma} \tag{C21}$$

Next

$$\cos \alpha' = \cos (\alpha + \theta) \cos \gamma + \sin (\alpha + \theta) \sin \gamma \cos x \tag{C22}$$

Substitution for cos x from Equation (C21) into Equation (C22) yields,

$$\cos \alpha' = - \frac{\cos \gamma \sin \alpha + \sin (\alpha + \theta) \cos \theta}{\sin \theta} \tag{C23}$$

Thus with Equation (C20), the angle α' is known in terms of α, θ, and φ.

Again application of the Spherical Law of Cosines gives

$$\cos y = \cos z \tag{C24}$$

and

$$\cos \theta = \cos \alpha \cos \alpha' + \sin \alpha \sin \alpha' \cos z \tag{C25}$$

Therefore,

$$\cos y = \frac{\cos \theta - \cos \alpha \cos \alpha'}{\sin \alpha \sin \alpha'} \tag{C26}$$

Now,

$$\beta' = \beta + y \tag{C27}$$

Therefore, between Equations (C23), (C26), and (C27) angle β' is known in terms of α, β, and φ.

From Equation (C7), the trigonometric identity for the sine of the sum of two angles produces

$$\sin \beta' = \sin \beta \cos y + \sin y \cos \beta \tag{C28}$$

At P then,

$$\sin \beta \cos y = -\sin y \cos \beta \tag{C29}$$

and

$$\cos y = \frac{\cos \theta_o}{\sin \alpha} \tag{C30}$$

$$\sin y = \pm \frac{\sqrt{\sin^2 \alpha - \cos^2 \theta_o}}{\sin \alpha} \tag{C31}$$

Between Equations (C29), (C30), and (C31), we obtain an expression for $\cos \theta_o$:

$$\cos \theta_o = \pm \sin \alpha \cos \beta \tag{C32}$$

Substitution for $\cos \theta_o$ in Equation (C30) results in

$$\cos y = \pm \cos \beta \tag{C33}$$

Therefore:

$$\sin y = \pm \sin \beta$$

At P since

$$\cos \alpha' = 0$$

we obtain for $\cos \gamma$ from Equation (C23):

$$\cos \gamma = \frac{\sin (\alpha + \theta_o) \cos \theta_o}{\sin \alpha} \tag{C34}$$

Between Equation (C34) and Equation (C20), we solve for $\cos \varphi_o$ and get

$$\cos \varphi_o = \frac{\cos \theta_o \cos \alpha}{\sin \theta_o \sin \alpha} = \pm \frac{\cos \alpha \cos \beta}{\sin \theta_o} \qquad \text{(C35)}$$

Then,

$$\sin \varphi_o = \pm \frac{\sin \beta}{\sin \theta_o} \qquad \text{(C36)}$$

We can now calculate the values of the derivatives in Equation (C14). Let,

$$\Delta_1 = \frac{\partial}{\partial \varphi} (\sin \beta' \sin \alpha') \Big]_{\substack{\theta = \theta_o \\ \varphi = \varphi_o}}$$

and

$$\Delta_2 = \frac{\partial}{\partial \varphi} (\cos \alpha') \Big]_{\substack{\theta = \theta_o \\ \varphi = \varphi_o}}$$

After considerable manipulation, we obtain

$$\Delta_1 = \pm \cos \alpha$$

$$\Delta_2 = - \frac{\cos \alpha}{\sin \theta_o}$$

Substitution into Equation (C14) with the knowledge that N = 2 (demonstrated below) results finally in

$$J = \frac{2 \sin^2 \theta_o}{\cos^2 \alpha} = 2 \frac{(1 - \sin^2 \alpha \cos^2 \beta)}{\cos^2 \alpha} \qquad \text{(C37)}$$

We must now show that N = 2. On the basis of the values of the sines and cosines of θ_o and φ_o, determined thus far, there are four possible points of contribution:

1) $\cos \theta_o = \sin \alpha \cos \beta$

$$\cos \varphi_o = \frac{\cos \alpha \cos \beta}{\sin \theta_o}$$

$$\sin \varphi_o = \frac{\sin \beta}{\sin \theta_o}$$

2) $\cos \theta_o = \sin \alpha \cos \beta$

$$\cos \varphi_o = \frac{\cos \alpha \cos \beta}{\sin \theta_o}$$

$$\sin \varphi_o = - \frac{\sin \beta}{\sin \theta_o}$$

3) $\cos \theta_o = - \sin \alpha \cos \beta$

$$\cos \varphi_o = - \frac{\cos \alpha \cos \beta}{\sin \theta_o}$$

$$\sin \varphi_o = \frac{\sin \beta}{\sin \theta_o}$$

4) $\cos \theta_o = - \sin \alpha \cos \beta$

$$\cos \varphi_o = - \frac{\cos \alpha \cos \beta}{\sin \theta_o}$$

$$\sin \varphi_o = - \frac{\sin \beta}{\sin \theta_o}$$

Since

$$0 \le \theta_o \le \pi$$

$$\sin \theta_o = + \sqrt{1 - \sin^2 \alpha \cos^2 \beta} > 0$$

At the allowed values of P,

$$\cos \beta' = 1$$

Therefore,

$$\cos \beta \cos y - \sin \beta \sin y = 1 \tag{C38}$$

In Equation (C38), for cos y we substitute

$$\cos y = \frac{\cos \theta_o}{\sin \alpha} = \pm \cos \beta$$

and for sin y,

$$\sin y = \pm \sin \beta$$

where it may be noted that $+\cos\beta$ corresponds to $\cos\theta_o = \sin\alpha\cos\beta$ and $-\cos\beta$ corresponds to $\cos\theta_o = -\sin\alpha\cos\beta$. After making all the possible substitutions, we have:

$$\cos^2\beta + \sin^2\beta = 1 \qquad \text{(a)}$$

$$\cos^2\beta - \sin^2\beta \neq 1 \qquad \text{(b)}$$

$$-\cos^2\beta - \sin^2\beta \neq 1 \qquad \text{(c)}$$

$$-\cos^2\beta + \sin^2\beta \neq 1 \qquad \text{(d)}$$

Since only condition (a) is allowed, this requires

$$\cos\theta_o = +\sin\alpha\cos\beta$$

$$\sin y = -\sin\beta$$

The last condition still permits two values of $\sin\varphi_o$; hence there are two allowed points of contribution. Then J in Equation (C37), in terms of velocity components, is

$$J = 2\left(\frac{v_z^{\,2} + v_\varphi^{\,2}}{v_z^{\,2}}\right) \tag{C39}$$

Integration over the second term of $\left(\frac{\partial f}{\partial t}\right)_{coll.}$ is trivial. The final result for the collision term is

$$\left(\frac{\partial f}{\partial t}\right)_{coll.} = \frac{g(v^2)\,h\,(r)}{r}\left[\frac{1}{2\pi\lambda v}\left(\frac{v_z^{\,2} + v_\varphi^{\,2}}{v_z^{\,2}}\right) - \frac{v}{\lambda}\,\delta(v_\varphi)\,\delta(v_z)\,h(v_r)\right] \tag{C40}$$

Next, to determine f we integrate along the characteristic. From Equation (C3)

$$df = -r\left(\frac{\partial f}{\partial t}\right)_{coll.}\frac{dv_\varphi}{v_\varphi v_r} \tag{C41}$$

The integration is performed under the condition that

$$rv_\varphi = \text{constant}$$

and

$$v_r = \sqrt{v_\perp^2 - v_\varphi^2}$$

The final result is obtained by making the constant of integration the no-collision distribution function of Equation (C4). This is permissible since this distribution function is a function only of constants of the motion (constants along the characteristic). Moreover, in this way the requirement that near the source, the effects of collision be negligible is satisfied. Then the result for the first iteration is

$$f = g(v^2)\Bigg[\left\{\frac{1}{r}\,\delta(v_\varphi)\,\delta(v_z)\,h(r)\,h(v_r)\right\} + \frac{1}{2\pi\lambda v}\left\{\frac{1}{2v_\perp}\,\ell n\left(\frac{v_\perp - \sqrt{v_\perp^2 - v_\varphi^2}}{v_\perp + \sqrt{v_\perp^2 - v_\varphi^2}}\right) + \frac{\sqrt{v_\perp^2 - v_\varphi^2}}{v_z^2}\right\} - \frac{v}{\lambda v_\perp^2}\left\{\delta(v_\varphi)\,\delta(v_z)\sqrt{v_\perp^2 - v_\varphi^2}\right\}\Bigg] \qquad \text{(C42)}$$

The electron number density is

$$\begin{aligned} n_e &= \int_{-\infty}^{\infty}\int_{-\infty}^{\infty}\int_{-\infty}^{\infty} f\,dv_z\,dv_\varphi\,dv_r \\ &= \int_0^\infty dv \int_0^\pi d\alpha \int_0^{2\pi} d\beta\, fv^2 \sin\alpha \end{aligned} \qquad \text{(C43)}$$

If one performs the indicated integration of Equation (C43), one obtains a zero contribution for the second term in Equation (C42). The remaining terms yield

$$n_e = \left(\frac{1}{r} - \frac{1}{\lambda}\right)\int_0^\infty g(v^2)\,dv \qquad \text{(C44)}$$

To continue the iteration process for the distribution function, one would substitute the first result, Equation (C42), into Equation (C5) and repeat the procedure previously followed. By inspection it can be seen that terms in $\frac{1}{\lambda^2}$ would be generated. Further inspection reveals that continued iteration will produce a power series in $\frac{1}{\lambda}$ as the effect of collision on both the distribution function and the number density.

2. Ions

For ions in three dimensions the Boltzmann equation, except for the detailed appearance of the scattering term, is similar to the electron equation. Consequently, the no-collision distribution function is similar:

$$f = \frac{F(v^2)}{r} \, \delta(v_\varphi)\, \delta(v_z)\, h(r)\, h(v_r) \tag{C45}$$

The collision term is different for ion-neutral collisions than for electron-neutral collisions even when we assume that both are isotropic in the center of mass system. The differences exist because the center of mass system and the laboratory system are different for ions. Also, in the laboratory system, there are transfers of energy from ions to neutrals during collision as a result of which ion speeds are altered (more than very slightly) by scattering. In what follows it will be assumed that the scattering is elastic, isotropic in the c. of m. system, and that the mass of ions and neutrals are equal. Further assumptions are that the speed of the ions before collisions is large compared to that of the neutrals and that the number of ions is sufficiently small so that the neutral distribution function is not appreciably disturbed. Under these conditions

$$\left(\frac{\partial f}{\partial t}\right)_{coll.} = \frac{v}{\pi\lambda} \int_0^{2\pi} \int_0^{\pi/2} (f' - f) \cos\theta \sin\theta \, d\theta \, d\varphi \tag{C46}$$

The range of integration over θ is zero to $\pi/2$ since scattering will be limited to the forward direction in the lab system for equal masses.

It is again convenient to work in a spherical coordinate system in order to relate the angles after collision to the angles before collision. The results are similar to that for the electrons except that now

$$v' = v \cos\theta$$

The results are summarized below:

$$
\begin{aligned}
v_z &= v \cos \alpha \\
v_r &= v \cos \beta \sin \alpha \\
v_\varphi &= v \sin \beta \sin \alpha \\
v_z{}' &= v \cos \theta \cos \alpha' \\
v_r{}' &= v \cos \theta \cos \beta' \sin \alpha' \\
v_\varphi{}' &= v \cos \theta \sin \beta' \sin \alpha'
\end{aligned}
\tag{C47}
$$

Now consider,

$$
\begin{aligned}
K &= \int_o^{2\pi} \int_o^{\pi/2} f' \cos \theta d\theta d\varphi \\
&= \frac{h(r)}{rv^2} \int_o^{2\pi} \int_o^{\pi/2} F(v'^2)\, \delta(\cos \theta \sin \beta' \sin \alpha') \cdot \\
&\qquad \delta(\cos \theta \cos \alpha')\, h(\cos \theta \cos \beta' \sin \alpha') \cdot \cos \theta \sin \theta d\theta d\varphi \\
&= \frac{h(r)}{rv^2} K
\end{aligned}
\tag{C48}
$$

Then,

$$
\begin{aligned}
K &= \int_o^{2\pi} \int_o^{\pi/2} F(v'^2) \frac{\delta(\theta - \theta_o)\, \delta(\varphi - \varphi_o)\, h(\cos \theta \cos \beta' \sin \alpha') \cos \theta \sin \theta d\theta d\varphi}{\left|\frac{\partial}{\partial \theta} (\cos \theta \cos \alpha')\right| \left|\frac{\partial}{\partial \varphi} (\cos \theta \sin \beta' \sin \alpha')\right|_{\substack{\varphi = \varphi_o \\ \theta = \theta_o}}} \\
&= \sum_{\substack{\varphi = \varphi_o \\ \theta = \theta_o}} \frac{\cos \theta_o \sin \theta_o F(v^2 \cos^2 \theta_o)}{\left|\frac{\partial}{\partial \theta} (\cos \theta \cos \alpha')\right| \left|\frac{\partial}{\partial \varphi} (\cos \theta \sin \beta' \sin \alpha')\right|_{\substack{\varphi = \varphi_o \\ \theta = \theta_o}}}
\end{aligned}
\tag{C49}
$$

where the summation is over all points where the arguments of the δ - functions in Equation (C4) vanish and where $\cos\theta \cos\beta' \sin\alpha' \geq 0$.

The value

$$\cos\theta = 0$$

gives only a zero contribution. As in the case of the electrons, the contributions are at $\cos\alpha' = 0$, $\sin\alpha' = 1$, $\sin\beta' = 0$, $\cos\beta' = 1$.

Then,

$$K = \sum_{\substack{\varphi=\varphi_o \\ \theta=\theta_o}} \frac{\sin^2\theta_o \, F(v^2\cos^2\theta_o)}{\cos\theta_o \cos^2\alpha}$$

But since

$$\cos\theta_o = \sin\alpha\cos\beta$$

and there are two contributions (as before),

$$K = \frac{2\,(1-\sin^2\alpha\cos^2\beta)}{\sin\alpha\left|\cos\beta\right|\cos^2\alpha} \, F(v^2\sin^2\alpha\cos^2\beta) \tag{C50}$$

Finally, in terms of velocity components,

$$K = \frac{2v\,(v^2 - v_r^{\,2})}{\left|v_r\right| v_z^{\,2}} \tag{C51}$$

Then the first term of $\left(\frac{\partial f}{\partial t}\right)_{coll.}$ is

$$\left(\frac{\partial f}{\partial t}\right)_1 = \frac{2}{\pi\lambda} \, F(v_r^{\,2}) \, \frac{h(r)}{r} \, \frac{1}{v_z^{\,2}} \, \frac{v_z^{\,2} + v_\varphi^{\,2}}{\sqrt{v^2 - v_\varphi^{\,2}}} \tag{C52}$$

Integration along the characteristic:

$$df_1 = \frac{r \left(\frac{\partial f}{\partial t}\right)_{coll.} dv_r}{v_\varphi^{\,2}} \tag{C53}$$

$$f_1 + C = \frac{2}{\pi\lambda} \frac{1}{v_z^{\,2}} \int \frac{F(v_r^{\,2})(v^2 - v_r^{\,2})\, dv_r}{v_r (v_\perp^{\,2} - v_r^{\,2})}$$

For the second term of $\left(\frac{\partial f}{\partial t}\right)_{coll.}$:

$$\left(\frac{\partial f}{\partial t}\right)_2 = - \frac{v}{\pi\lambda} f \int_0^{2\pi} \int_0^{\pi/2} \cos\theta \sin\theta d\theta d\varphi = - \frac{v}{\lambda} f \tag{C54}$$

For this term integration along the characteristic yields, when f is taken to be approximated by the no-collision distribution function,

$$f_2 + C = - \frac{1}{\lambda} F(v^2)\, \delta(v_\varphi)\, \delta(v_z) \frac{|v_r|}{v} \tag{C55}$$

Combining these results we get

$$f = \left\{ \frac{h(r)\, h(v_r)}{r} - \frac{1}{\lambda} \frac{|v_r|}{v} \right\} F(v^2)\, \delta(v_\varphi)\, \delta(v_z)$$

$$+ \frac{2}{\pi\lambda} \frac{1}{v_z^{\,2}} \int \frac{F(v_r^{\,2})(v^2 - v_r^{\,2})}{v_r (v_\perp^{\,2} - v_r^{\,2})} dv_r \tag{C56}$$

Therefore in the case of the ions the form of the distribution function can only be given in terms of an indefinite integral.

D. RADIAL CHARGE SEPARATION NEGLECTING COLLISIONS

The effect of charge separation as a result of differences in inertia and source function for the ions and electrons is to produce a radial field. The kinetic equation describing the particle distribution is:

$$rv_r \frac{\partial f}{\partial r} - v_\varphi v_r \frac{\partial f}{\partial v_\varphi} + \left(v_\varphi^{\,2} + \frac{qE}{m} r \right) \frac{\partial f}{\partial v_r} = 0 \tag{D1}$$

Here q is the charge of the particle having the value +e for the ions and -e for the electrons, while m has the value m_i for the ions and m_e for the electrons. The field E is purely radial. Coupled to this equation is Poisson's equation:

$$\nabla^2 V = -\frac{\rho}{\epsilon_o} \tag{D2}$$

where V is the potential, ρ is the charge density and ϵ_o is the permittivity of free space. The potential is related to the field by the equation:

$$V = -\int_o^r E\,dr \tag{D3}$$

and ρ is obtained from the distribution functions by the equation

$$\rho = e \left[\int_{-\infty}^{\infty} \int_{-\infty}^{\infty} f_i \, dv_r \, dv_\varphi - \int_{-\infty}^{\infty} \int_{-\infty}^{\infty} f_e \, dv_r \, dv_\varphi \right] \tag{D4}$$

where f_i and f_e are the ion and electron distributions respectively.

Using the method of characteristics, as before, we find the differential equations describing the characteristic curves (which in the no-collision approximation are the trajectories of the particles). These are:

$$\frac{dr}{rv_r} = -\frac{dv_\varphi}{v_\varphi v_r} = \frac{dv_r}{v_\varphi^{\,2} + \frac{qE}{m} r} \tag{D5}$$

Integrating the equation formed by the first two terms on the left, we find that:

$$rv_\varphi = C, \text{ a constant} \tag{D6}$$

From the first and third terms and the constancy of $r v_\varphi$ we obtain:

$$\frac{dr}{r} = \frac{v_r \, dr}{\left(\frac{C}{r}\right)^2 + \frac{qE}{m} r} \tag{D7}$$

Integrating Equation (D7)

$$\int dr \left[\frac{C}{r^3} + \frac{qE}{m}\right] = \int v_r \, dv_r - \frac{C}{2r^2} + \frac{q}{m}\int E\,dr = \frac{v_r^2}{2} + C' \tag{D8}$$

Replacing C by rv_φ and C' by

$$\frac{v_o^2}{2},$$

and letting

$$v^2 = v_\varphi^2 + v_r^2 \tag{D9}$$

we obtain

$$v_o^2 = v^2 - \frac{2q}{m}\int_o^r E dr \tag{D10}$$

which is merely a statement of the conservation of energy where v_o^2 is proportional to the energy of the particle at the source and is a constant along the characteristic.

We must now construct a distribution function which is a function of the constants rv_φ^2 and v_o^2 and reduces to the no-field distribution function near the source $(r \to o)$. The no-field distribution functions for electrons and ions are:

$$\begin{aligned} f_e &= \frac{1}{r}\, \delta(v_\varphi)\, h(r)\, h(v_r)\, g(v^2) \\ f_i &= \frac{1}{r}\, \delta(v_\varphi)\, h(r)\, h(v_r)\, F(v^2) \end{aligned} \tag{D11}$$

where the h's are unit step functions.

With the field the proper distribution functions are:

$$f_e = \frac{1}{r}\,\delta(v_\varphi)\,h(r)\,h(v_{roe})\,g(v_{oe}^2)$$

$$f_i = \frac{1}{r}\,\delta(v_\varphi)\,h(r)\,h(v_{roi})\,F(v_{oi}^2) \tag{D12}$$

where:

$$v_{oe}^2 = v^2 + \frac{2e}{m_e}\int_o^r Edr$$

$$v_{oi}^2 = v^2 - \frac{2e}{m_i}\int_o^r Edr \tag{D13}$$

Now to obtain an explicit solution it is necessary to solve for the field E. The number density of electrons is given by:

$$n_e = \frac{1}{r}\int_{-\infty}^{\infty}\int_{\infty}^{\infty}\delta(v_\varphi)\,g(v_o^2)\,h(v_{ro})\,h(r)\,dv_\varphi\,dv_r$$

$$= \frac{1}{r}\int_{-\pi}^{\pi}\int_o^v \delta(\sin\alpha)\,g(v_o^2)\,dv\,d\alpha \tag{D14}$$

where α is the angle between the velocity vector and v_r, the radial component of the velocity. Integrating over α

$$n_e = \frac{1}{r}\int_{v_{min}}^{\infty} g(v_o^2)\,h(v_{ro})\,dv \tag{D15}$$

where v_{min} corresponds to $v_o = 0$. Then we transform to v_o as the variable of integration.

$$n_e = \frac{1}{r}\int_o^{\infty} g(v_o^2)\left(\frac{dv}{dv_o}\right) dv_o = \frac{1}{r}\int_o^{\infty}\frac{g(v_o^2)\,v_o\,dv_c}{\sqrt{v_o^2 - \frac{2e}{m_e}\int_o^r Edr}} \tag{D16}$$

Similarly:

$$n_i = \frac{1}{r} \int_0^{\infty} \frac{F(v_o^2)\, v_o\, dv_o}{\sqrt{v_o^2 + \frac{2e}{m_i} \int_0^r E dr}} \tag{D17}$$

and the charge density is given by:

$$\rho = e(n_i - n_e) = \frac{e}{r} \left[\int_0^{\infty} \frac{F(v_o^2)\, v_o\, dv_o}{\sqrt{v_o^2 - \frac{2e}{m_i} V}} - \int_0^{\infty} \frac{g(v_o^2)\, v_o\, dv_o}{\sqrt{v_o^2 + \frac{2e}{m_e} V}} \right] \tag{D18}$$

If we substitute Equation (D18) into Equation (D2) and solve the resulting non-linear differential equation for V, then we have an explicit solution.

The general solution requires numerical methods; however, for distances near the source and also distances very far from the source, approximate analytic solutions may be obtained. Near the source, as a first approximation the effect of the field on the distribution of particles may be considered small. This is equivalent to neglecting $2eV/m$ compared to v_o^2 for most values of v_o^2 in the integrals of Equation (D18). Then the charge density is given by·

$$\rho = \frac{e}{r} [C - B] \tag{D19}$$

where C and B are constants

$$C \equiv \int_0^{\infty} F(v_o^2)\, dv_o$$

$$B = \int_0^{\infty} g(v_o^2)\, dv_o \tag{D20}$$

From Gauss' Law:

$$2\pi r E = \frac{1}{\epsilon_o} \int_0^r 2\pi \rho r' dr'$$

or

$$E = \frac{1}{\epsilon_o r} \int_0^r \rho r' dr' \tag{D21}$$

Then from Equation (19)

$$E = \frac{e}{\epsilon_o} \left[C - B \right] \tag{D22}$$

Therefore near the origin the radial field is approximately constant.

For the asymptotic solution far from the source, let us assume that for r large, $V \to V_o - F(r)$ where $F(r) \to 0$ for $r \to \infty$ and V_o is the value of V which corresponds to $\rho = 0$. Then V_o satisfies the equation

$$\int_o^\infty \frac{F(v_o^2)\, v_o\, dv_o}{\sqrt{v_o^2 - \frac{2e}{m_i} V_o}} - \int_o^\infty \frac{g\,(v_o^2)\, v_o\, dv_o}{\sqrt{v_o^2 + \frac{2e}{m_e} V_o}} = 0 \tag{D23}$$

If we expand the denominator appearing in Equation (18) for small F(r), we obtain:

$$\frac{1}{\sqrt{v_o^2 - \frac{2e}{m_i} V}} \approx \frac{1}{\sqrt{v_o^2 - \frac{2e}{m_i} V_o}} \left[1 + \frac{\frac{e}{m_i} F(r)}{v_o^2 - \frac{2eV_o}{m_i}} \right]$$

$$\frac{1}{\sqrt{v_o^2 + \frac{2e}{m_e} V}} \approx \frac{1}{\sqrt{v_o^2 + \frac{2e}{m_e} V_o}} \left[1 - \frac{\frac{e}{m_e} F(r)}{v_o^2 + \frac{2eV_o}{m_e}} \right] \tag{D24}$$

Making use of Equations (D2), (D18), (D23), and (D24), we derive the following linear equation for F:

$$\frac{d}{d_r} \left(r \frac{d_F}{d_r}\right) = -AF \tag{D25}$$

where A is a positive constant given by:

$$A = \frac{e}{\epsilon_o} \left[\frac{e}{m_i} \int_o \frac{F(v_o^{\,2})\, v_o\, dv_o}{\left\{ v_o^{\,2} - \frac{2e}{m_i} V \right\}^{3/2}} + \frac{e}{m_e} \int_o^{\infty} \frac{g(v_o^{\,2}) v_o\, dv_o}{\left\{ v_o^{\,2} + \frac{2e}{m_e} V_o \right\}^{3/2}} \right]$$

(D26)

The solution of Equation (D25) is made easier by change of independent variable. Let:

$$F(r) = G(x) \tag{D27}$$

where

$$x = Ar \tag{D28}$$

Then Equation (D25) becomes:

$$x \frac{d^2G}{dx^2} + \frac{dG}{dx} + G = 0 \tag{D29}$$

If we let g be the Laplace Transform of G and p the transform variable, the transformed equation becomes:

$$p^2 \frac{dg}{dp} + (p-1)g = 0 \tag{D30}$$

Therefore,

$$-\frac{dg}{g} = \left(\frac{1}{p} - \frac{1}{p^2} \right) dp \tag{D31}$$

Integrating Equation (D31), we find:

$$g = K e^{-\frac{1}{p}} \tag{D32}$$

where K is a constant of integration. Inversion of the Laplace Transform yields:

$$G = K\, J_o\, (2x^{\frac{1}{2}}) \tag{D33}$$

where J_o is Bessel's function of the first kind.

If we let:

$$y = 2x^{\frac{1}{2}}$$

and

$$G(x) = Q(y) \tag{D34}$$

and if we substitute in Equation (D29), we obtain:

$$\frac{d^2Q}{dy^2} + \frac{1}{y}\frac{dQ}{dy} + Q = 0 \tag{D35}$$

This is immediately recognizable as Bessel's Equation of Zero order. This equation has two independent solutions. As a result, the general solution for F is:

$$F = aJ_o\left(2\left[Ar\right]^{\frac{1}{2}}\right) + b\,N_o\left(2\left[Ar\right]^{\frac{1}{2}}\right) \tag{D36}$$

where No is the Neumann function of zero order. Since this result holds for r large, we may use the asymptotic expansions of the Bessel functions to write:

$$F \approx \frac{1}{r^{\frac{1}{4}}}\left[a\cos\left(2\left[Ar\right]^{\frac{1}{2}}\right) + b\sin\left(2\left[Ar\right]^{\frac{1}{2}}\right)\right]$$

Therefore, for large r, the potential oscillates about V_o with the oscillation decaying slowly as $r^{-1/4}$. This implies further that the charge density oscillates passing through periodic changes in sign.

E. ELECTRON AND ION DISTRIBUTION FUNCTIONS IN A UNIFORM EXTERNAL FIELD.

The stationary collisionless Boltzmann equation is

$$\underline{v} \cdot \nabla f + \frac{\underline{F}}{m} \cdot \nabla_v f = 0 \tag{E1}$$

where $\underline{v}$ is the particle velocity, $\underline{F}$ is a force field and m is the particle mass. Let

$$\underline{F} = \underline{F_o} + \underline{F_1} \tag{E2}$$

where $\underline{F_o}$ is externally imposed and $\underline{F_1}$ is a result of the redistribution of particles. The distribution f may be written as

$$f = f_o + f_1 \tag{E3}$$

where f_o is the distribution which would result if $\underline{F_o}$ were the only force field present, and

$$\underline{v} \cdot \nabla f_o + \frac{\underline{F_o}}{m} \cdot \nabla_v f_o = 0 \tag{E4}$$

Then from equation (E1), (E2), (E3) and (E4) and the assumption that $\frac{\underline{F_1}}{m} \cdot \nabla_v f_1$ is negligible, it follows that

$$\underline{v} \cdot \nabla f_1 + \frac{\underline{F_o}}{m} \cdot \nabla_v f_1 = \frac{-\underline{F_1}}{m} \cdot \nabla_v f_o \tag{E5}$$

Now if $\underline{F} = q\underline{E} = q(\underline{E_o} + \underline{E_1})$ with $q = e$ tor ions and $-e$ for electrons and $\underline{E_o}$ is a uniform external electric field, then one can define a potential such that

$$\underline{E_o} = -\nabla V_o \tag{E6}$$

and

$$\underline{E_1} = -\nabla V_1$$

Then these potentials satisfy the equations

$$\nabla^2 V_o = 0$$

$$\nabla^2 V_1 = \frac{-e}{\epsilon_o}\left[\int f_{io}\, d^3_v - \int f_{eo}\, d^3_v\right] \tag{E7}$$

where f_{eo} and f_{io} are the zero order electron and ion distributions. We will now carry the analysis through the solution of equation (E4) for the determination of f_o and the subsequent solution of equation (E7) for the determination of $\underline{E_1}$

In cylindrical coordinates equation (E1) or equation (E4) may be written as

$$rv_r \frac{\partial f}{\partial r} + v_\varphi \frac{\partial f}{\partial \varphi} + \frac{\partial f}{\partial v_r}\left(v_\varphi^{\ 2} + \frac{rq}{m} E_r\right) +$$

$$\frac{\partial f}{\partial v_\varphi}\left(-v_\varphi v_r + \frac{rq\, E\varphi}{m}\right) = 0 \tag{E8}$$

The differential equations for the characteristics are therefore

$$\frac{dr}{rv_r} = \frac{d\varphi}{v_\varphi} = \frac{dv_r}{\left(v_\varphi^{\ 2} + \frac{rq}{m} E_r\right)} = \frac{dv_\varphi}{\left(-v_\varphi v_r + \frac{rq}{m} E_\varphi\right)} \tag{E9}$$

It can readily be shown that the characteristics for the collisionless Boltzmann equation are also the trajectories of the particles in the given field. From the second and fourth terms of equation (E9) we obtain

$$\left(-v_\varphi v_r + \frac{rq}{m} E_\varphi \right) d\varphi = v_\varphi \, dv_\varphi \tag{E10}$$

From the first and third terms, we obtain

$$\left(\frac{v_\varphi^2}{r} + \frac{q}{m} E_r \right) dr = v_r \, dv_r \tag{E11}$$

but since

$$\frac{dr}{r} = d\varphi \, \frac{v_r}{v_\varphi}$$

substitution in equation (E11) yields

$$v_\varphi v_r \, d\varphi + \frac{q}{m} E_r \, d_r = v_r \, dv_r \tag{E12}$$

Addition of equation (E10) and (E12) yields

$$\frac{q}{m} \left(rE_\varphi \, d\varphi + E_r \, d_r \right) = v_\varphi \, dv_\varphi + v_r \, dv_r \tag{E13}$$

Integration of equation (E13) finally results in

$$v^2 = v_o^2 + \frac{2q}{m} \left[\int_o^r E_r \, dr + \int_{\varphi_i}^{\varphi} rE_\varphi \, d\varphi \right] \tag{E14}$$

Here equation (E14) is simply an expression of the fact that the energy of the particle is the original energy $\frac{1}{2} m v_o^2$ plus the work done on the particle by the electric field.

If the field is in the x direction, then

$$E_r = E_o \cos \varphi$$

$$E_\varphi = -E_o \sin \varphi \tag{E15}$$

For this case it can be shown that v_y is a constant along a characteristic, a result which, of course, also follows immediately from Newton's First Law.

A solution of equation (E4) is any function of those quantities which are constants along the characteristics. In addition, we choose the solution such that near the origin, it goes to the zero field limit. Let the subscript zero designate the value at the origin. Then the distribution function is

$$f = \delta \left(rv_\varphi \right)_o g \left(v_o^2 \right) h \left(r_o \right) h \left(v_{r_o} \right) \tag{E16}$$

for the electrons. For the ions $\underline{F} (v_o^2)$ replaces $g (v_o^2)$.

Since we are taking the initial values just outside the source $h (r_o) h (v_{ro})$ is redundant. We need only find $(rv_\varphi)_o$, and v_o in terms of r, φ, v_r and v_φ or any equivalent coordinate system to obtain solution.

Now

$$rv_\varphi = xv_y - yv_x \tag{E17}$$

and

$$(rv_\varphi)_o = rv_\varphi - \int_{to}^{t} \frac{d}{dt} (xv_y - yv_x) dt \tag{E18}$$

Since v_y is constant on the characteristic

$$(rv_\varphi)_o = xv_y - yv_x + \int_{to}^{t} y\dot{v}_x dt \tag{E19}$$

But

$$\dot{v}_x = \frac{qE}{m}$$

where for simplicity we have dropped the subscripts from E_{ox}. If we make use of the fact that

$$dy = v_y \, dt$$

and that $y_o = 0$, we can show that

$$\delta\left(\left\{rv_\varphi\right\}_o\right) = \frac{1}{y}\,\delta\left(v_x - v_y\frac{x}{y} + \frac{qE}{2m}\,\frac{y}{v_y}\right) \qquad \text{(E20)}$$

In $g(v_o^2)$ or $\underline{F}(v_o^2)$

$$v_o^2 = v_x^2 + v_y^2 - \frac{2q}{m}\,Ex \qquad \text{(E21)}$$

The number density of electrons is then

$$n_e = \int_{-\infty}^{\infty}\int_{-\infty}^{\infty} \frac{1}{y}\,\delta\left(v_x - v_y\frac{x}{y} + \frac{qE}{2m}\,\frac{y}{v_y}\right) g(v_o^2)\, dv_x\, dv_y \qquad \text{(E22)}$$

If we integrate over dv_x

$$n_e = \int_{-\infty}^{\infty} \frac{1}{y}\, g\,(v_o^2)\, dv_y \qquad \text{(E23)}$$

where in the expression of equation (E21)

$$v_x = v_y\frac{x}{y} - \frac{qE}{2m}\,\frac{y}{v_y} \qquad \text{(E24)}$$

Now

$$v_o^2 = v_y^2 \left(1 + \frac{x^2}{y^2} \right) + \left(\frac{qE}{2m} \right)^2 \frac{y^2}{v_y^2} - \frac{3qE}{m} x \qquad \text{(E25)}$$

We need the solution of v_y in terms of v_o and the other variables. This is

$$v_y = \left[\frac{v_o^2 + \frac{3qE}{m} x + \sqrt{v_o^4 + 8\left(\frac{qE}{m}\right)^2 x^2 + \frac{6qE}{m} v_o^2 x - \left(\frac{qE}{m}\right)^2 y^2}}{2\left(1 + \frac{x^2}{y^2} \right)} \right]^{\frac{1}{2}} \qquad \text{(E26)}$$

The integral in equation (E23) can be transformed to

$$n_e = \int_{-\infty}^{\infty} \frac{1}{y} \, g\,(v_o^2) \left(\frac{dv_y}{dv_o} \right) dv_o \qquad \text{(E27)}$$

The required derivative from equation (E26) is

$$\frac{dv_y}{dv_o} = \frac{1}{2^{\frac{1}{2}}} \frac{y v_o}{x^2 + y^2} \; \frac{\left(\bar{X} + v_o^2 + \frac{3qE}{m} x \right)^{\frac{1}{2}}}{\bar{X}} \qquad \text{(E28)}$$

where

$$\bar{X} = \sqrt{v_o^4 + 8 \left(\frac{qE}{m}\right)^2 x^2 + \frac{6qE}{m} v_o^2 x - \left(\frac{qE}{m}\right)^2 y^2} \qquad \text{(E29)}$$

Thus, in principle, if $g\,(v_o^2)$ is a known function, the integration of equation (E27) can be completed.

If $\frac{qE}{m}$ is a small quantity so that

$$\frac{qE}{m} \frac{x}{v_o^2}$$

and

$$\frac{qE}{m} \frac{y}{v_o^2}$$

are small compared to unity, then

$$n_e \approx \frac{1}{r} \int_{-\infty}^{\infty} g\,(v_o^2)\,\left(1 - \frac{3}{2} \frac{qE}{m} \frac{x}{v_o^2} \right) dv_o \tag{E30}$$

For this approximation to be valid, the function $g(v_o^2)$ must be such as to give a sizeable contribution to the integral only for

$$v_o^2 \gg \frac{qE}{m} x \tag{E31}$$

Then

$$n_e = \frac{1}{r} \left[\int g\,(v_o^2)\, dv_o - \frac{3}{2m} qEx \int \frac{g\,(v_o^2)}{v_o^2} dv_o \right] \tag{E32}$$

so that the effect of the uniform field is to alter the particle density by the amount of the second term.

We will now consider the case where the above approximation is also valid for the ions, and where the electron and ion source distributions have a particularly simple form:

$$g\,(v_o^2) = A\, v_o^2\, \delta\,(v_o - v_e)$$

$$F\,(v_o^2) = B\, v_o^2\, \delta\,(v_o - v_i) \tag{E33}$$

The the charge density ρ is given by

$$\rho = e(n_i - n_e) = \frac{e}{r}\left[Bv_i^2 - Av_e^2 - \frac{3}{2} eEx \left(\frac{B}{m_i} + \frac{A}{m_e}\right)\right] \quad \text{(E34)}$$

In the present example Poisson's equation becomes

$$\frac{1}{r}\frac{\partial}{\partial r}\left(r\frac{\partial v}{\partial r}\right) + \frac{1}{r^2}\frac{\partial v}{\partial \varphi^2} = -\frac{H}{r} + G\cos\varphi \quad \text{(E35)}$$

where

$$H = \frac{e}{\epsilon_o}(Bv_i^2 - Av_e^2)$$

and

$$G = \frac{3}{2}\frac{e^2}{\epsilon_o} E \left(\frac{B}{m_i} + \frac{A}{m_e}\right)$$

The appropriate solution of equation (E35) is

$$V = -H_r + \frac{G_r^2}{3}\cos\varphi \quad \text{(E36)}$$

where the first term on the right is the result of radial charge separation and the second term is the effect of the imposed uniform field.

Therefore the field induced by the redistribution of charge is

$$E_{1x} = -\frac{\partial v}{\partial x} = \frac{1}{2}\frac{e^2}{\epsilon_o} E \left(\frac{B}{m_i} + \frac{A}{m_e}\right)\left[\frac{2x^2 + y^2}{(x^2 + y^2)^{\frac{1}{2}}}\right] \quad \text{(E37)}$$

$$E_{1y} = -\frac{\partial v}{\partial y} = \frac{1}{2}\frac{e^2}{\epsilon_o} E \left(\frac{B}{m_i} + \frac{A}{m_e}\right)\left[\frac{x_y}{(x^2 + y^2)^{\frac{1}{2}}}\right]$$

It may be noted that at the source (electron beam) where $(x, y) = (o, o)$, the induced fields are zero. Hence at this location only the imposed uniform field is present.

PRECEDING PAGE BLANK NOT FILMED.

APPENDIX II

To check the validity of the assumption of Equation (13), namely,

$$\lambda_j = \lambda_{N/4} \sin \frac{2\pi j}{N} \qquad -1$$

we substitute this expression for λ_j into Equation (12) and check to see whether the equation is satisfied. To make the substitution we must evaluate the summation Σ_k where

$$\Sigma_k = \sum_{\substack{j=0 \\ j\neq k}}^{N/2} \sin \frac{2\pi j}{N} \ln \left[\frac{\sin(j+k)(\pi/N)}{|\sin(j-k)(\pi/N)|} \right] \qquad -2$$

We break the sum into a number of partial sums as follows:

$$\Sigma_k = \sum_{j=0}^{k-1} \sin \frac{2j\pi}{N} \ln \left[\sin(j+k) \frac{\pi}{N} \right] + \sum_{j=k+1}^{N/2} \sin \frac{2j\pi}{N} \ln \left[\sin(j+k) \frac{\pi}{N} \right]$$

$$- \sum_{j=0}^{k-1} \sin \frac{2j\pi}{N} \ln \left| \sin(j-k) \frac{\pi}{N} \right| - \sum_{j=k+1}^{N/2} \sin \frac{2j\pi}{N} \ln \left| \sin(j-k) \frac{\pi}{N} \right| \qquad -3$$

Now, if we approximate integrals for summations, we obtain for the first summation

$$I_1 = \sum_{j=0}^{k-1} \sin \frac{2j\pi}{N} \ln \left[\sin(j+k) \frac{\pi}{N} \right] \simeq \int_0^{k-1} \sin \frac{2j\pi}{N} \ln \left[\sin(j+k) \frac{\pi}{N} \right] dj \qquad -4$$

If we make use of the transformation

$$s = (j+k) \frac{\pi}{N}$$

I_1 becomes

$$I_1 \simeq \int_{\frac{k\pi}{N}}^{(2k-1)\frac{\pi}{N}} \sin \left(2s - \frac{2k\pi}{N} \right) \ln \sin s ds \qquad -5$$

In all the terms in Equation (3) are treated similarly with the transformation

$$s = (j-k) \frac{\pi}{N}$$

being used in the second two terms, we obtain, finally,

$$k = \frac{N}{\pi}\left[\cos\frac{2k\pi}{N}\left\{\int_{\frac{k\pi}{N}}^{(2k-1)\frac{\pi}{N}} Fds + \int_{(2k+1)\frac{\pi}{N}}^{(\pi/2)+(k\pi/N)} Fds - \int_{\frac{-k\pi}{N}}^{-\pi/N} Fds - \int_{\frac{\pi}{N}}^{(\pi/2)-(k\pi/N)} Fds\right\}\right.$$

$$\left. -\sin\frac{2k\pi}{N}\left\{\int_{\frac{k\pi}{N}}^{(2k-1)\frac{\pi}{N}} Gds + \int_{(2k+1)\frac{\pi}{N}}^{(\pi/2)+(k\pi/N)} Gds + \int_{\frac{-k\pi}{N}}^{-\pi/N} Gds + \int_{\frac{\pi}{N}}^{(\pi/2)-(k\pi/N)} Gds\right\}\right]$$ -6

where

$$F = \sin 2t \ln|\sin t|$$

$$G = \cos 2t \ln|\sin t|$$ -7

Now

$$\int Fds = (\sin^2 s)(\ln|\sin s| - \tfrac{1}{2})$$

$$\int Gds = \tfrac{1}{2}\left\{(\sin 2s)(\ln|\sin s| - \tfrac{1}{2}) - s\right\}$$ -8

We now evaluate Equation (6) and obtain

$$\Sigma_k \simeq \frac{N}{\pi}\left[-\sin(2k+1)\frac{\pi}{N}\sin\frac{\pi}{N}\left\{\ln\sin(2k+1)\frac{\pi}{N} - \tfrac{1}{2}\right\}\right.$$

$$-\sin(2k-1)\frac{\pi}{N}\sin\frac{\pi}{N}\left\{\ln\sin(2k-1)\frac{\pi}{N} - \tfrac{1}{2}\right\}$$

$$\left.+\sin\frac{2k\pi}{N}\sin\frac{2\pi}{N}\left\{\ln\sin\frac{\pi}{N} - \tfrac{1}{2}\right\} - \tfrac{1}{2}\sin\frac{2k\pi}{N}\left(\frac{2\pi}{N} - \pi\right)\right]$$

Then, if we neglect terms of 0(1/N) compared to terms of 0(1)

$$\Sigma_k \simeq \frac{N}{2}\sin\frac{2k\pi}{N}$$ -9

It may immediately be noted that for k = N/4, the result of Equation (20) is obtained. We now substitute into Equation(12)and solve for λ_k. The result is

$$\lambda_k = \lambda_{N/4}\sin\frac{2k\pi}{N}\left[\frac{1}{1 + \dfrac{\ln\sin\frac{2k\pi}{N}}{\ln\left(\frac{2R}{\rho}\right)}}\right]$$ -10

Therefore, the assumption of Equation (13) is valid except where k is small, i.e., near $y = \pm R$. Since the λ_j's are small here, they make only a small contribution to the summation of Equation (16); hence, the error produced by the assumption of Equation (12) is small.